Naval Research Laboratory

Washington, DC 20375-5320

NRL/MR/6180--11-9318

Liquid Loss From Advancing Aqueous Foams With Very Low Water Content

MICHAEL CONROY
RAMAGOPAL ANANTH
JAMES FLEMING
JUSTIN TAYLOR
JOHN FARLEY

Navy Technology Center for Safety and Survivability
Chemistry Division

January 14, 2011

REPORT DOCUMENTATION PAGE

Form Approved
OMB No. 0704-0188

1. REPORT DATE *(DD-MM-YYYY)*	**2. REPORT TYPE**	**3. DATES COVERED** *(From - To)*
14-01-2011	Memorandum Report	

4. TITLE AND SUBTITLE

Liquid Loss From Advancing Aqueous Foams With Very Low Water Content

5a. CONTRACT NUMBER

5b. GRANT NUMBER

5c. PROGRAM ELEMENT NUMBER

6. AUTHOR(S)

Michael Conroy, Ramagopal Ananth, James Fleming,
Justin Taylor, and John Farley

5d. PROJECT NUMBER

5e. TASK NUMBER

5f. WORK UNIT NUMBER

7. PERFORMING ORGANIZATION NAME(S) AND ADDRESS(ES)

Naval Research Laboratory, Code 6180
4555 Overlook Avenue, SW
Washington, DC 20375-5320

8. PERFORMING ORGANIZATION REPORT NUMBER

NRL/MR/6180--11-9318

9. SPONSORING / MONITORING AGENCY NAME(S) AND ADDRESS(ES)

Office of Naval Research
One Liberty Center
875 North Randolph Street Suite 1425
Arlington, VA 22203-1995

10. SPONSOR / MONITOR'S ACRONYM(S)

11. SPONSOR / MONITOR'S REPORT NUMBER(S)

12. DISTRIBUTION / AVAILABILITY STATEMENT

Approved for public release; distribution is unlimited.

13. SUPPLEMENTARY NOTES

14. ABSTRACT

Applications employing aqueous foams begin with filling a space with foam, and the liquid loss (drainage) from the foam during and after this process plays a crucial role in its effectiveness. We describe the loss of liquid from foam and the evolution of its average liquid fraction over time. The theoretical model shows a constant drainage rate during the filling process which decays exponentially after a static column is formed. Modeling the advancing foam front requires a new time scale, the fill time, which substantially affects the drainage of liquid. Significant effects are also found by varing bubble size, foam column height, and initial expansion ratio, i.e., the volume ratio of foam to liquid. Foams with low water content are generated experimentally at the bench scale, and the measured loss of liquid is found to be in good agreement with the theoretical predictions.

15. SUBJECT TERMS

High expansion foam
Aqueous foams
Fire suppression
Drainage

16. SECURITY CLASSIFICATION OF:			**17. LIMITATION OF ABSTRACT**	**18. NUMBER OF PAGES**	**19a. NAME OF RESPONSIBLE PERSON**
a. REPORT	**b. ABSTRACT**	**c. THIS PAGE**			Ramagopal Ananth
Unclassified	Unclassified	Unclassified	UL	62	**19b. TELEPHONE NUMBER** *(include area code)* (202) 767-3197

CONTENTS

1.0 INTRODUCTION 1

2.0 MODEL 4

3.0 EXPERIMENTS 27

4.0 RESULTS AND DISCUSSION 31

5.0 CONCLUSIONS 49

6.0 ACKNOWLEDGMENTS 50

7.0 REFERENCES 50

APPENDIX A - Calculation of the superficial liquid velocity for a cylindrical channel 52

APPENDIX B – Model parameters for comparison with Reference [8] 56

NOMENCLATURE

A, characteristic drainage constant, m/s

a_p, cross-sectional area of channel (Plateau border), m^2

B, characteristic drainage constant, m^2/s

C_1, integration constant

C_2, integration constant

c_v, parameter to account for the mobility of channel walls; defined as the ratio of the average liquid velocity in a given channel with mobile walls to the average liquid velocity in the same channel if the walls are immobile, dimensionless

D_b, diameter of a bubble, m

Ex, foam expansion ratio, dimensionless

G, geometrical constant equal to $(15+7\sqrt{5})/4 \approx 7.66$, dimensionless

g, gravitational acceleration, $9.8\, m/s^2$

H, height of foam column, m

h_f, height of moving boundary at the top of the foam, m

h_{f0}, initial height of the top of the foam, m

h_w, height of the moving boundary at the top of the liquid layer beneath the foam, m

h_{w0}, initial height of the top of the liquid layer beneath the foam, m

L, channel (Plateau border) length, m

M_d, mass of liquid drained from the foam, kg

n_p, number of channels (Plateau borders) per bubble, #

P_g, pressure of gas in bubble, Pa

P_l, pressure of liquid in a channel (Plateau border), Pa

r, radius of curvature of the interface between a gas bubble and a liquid channel, m

R, radius of cylindrical foam column, m

S, cross-sectional area of foam column, m^2

t, time, s

t_0, initial time, s

t_{ind}, induction time, s

t_{fill}, time required to fill a column with foam, s

V_b, volume of gas within a bubble, m^3

V_d, volume of liquid drained from a foam, m^3

v, liquid velocity within a channel averaged over the cross-section of a channel (Plateau border), m/s

$\overline{v}$, liquid velocity within a channel averaged over the height of the foam layer, m/s

v_{inj}, injection velocity of foam, m/s

v_s, superficial liquid velocity, m/s

z, vertical coordinate along the height of the foam column, m

GREEK SYMBOLS

α, liquid volume fraction of foam, dimensionless

$\overline{\alpha}$, liquid volume fraction of foam averaged over the height of the foam layer, dimensionless

α_f, liquid volume fraction of foam injected into foam column, dimensionless

α_w, liquid volume fraction at the interface between the foam and drained liquid layers, dimensionless

γ, surface tension, $0.0225\ N/m$

δ, model constant equal to approximately 0.21, dimensionless

δ_a, model constant equal to $\sqrt{3} - \pi / 2 \approx 0.161$, dimensionless

η, reciprocal (multiplicative inverse) of $\bar{\alpha}$, dimensionless

θ, model constant for comparing foam drainage models, dimensionless

μ, viscosity of liquid, $0.000893\ kg / ms$

ξ, permeability coefficient, dimensionless

ρ, mass density of liquid, $997\ kg / m^3$

Φ, generic function in the standard form of a linear ordinary differential equation

ψ, generic integration factor used in the analytical solution of a linear ordinary differential equation

Ω, generic function in the standard form of linear ordinary differential equation

Liquid Loss from Advancing Aqueous Foams with Very Low Water Content

1.0 INTRODUCTION

Filling a space with foam is an essential part of foam applications. One filling method is to apply foam directly onto a surface from above, where fresh foam is added to the top of the advancing foam bed. This method of filling is used, for example, in fire-suppression applications. To suppress fires in contained spaces such as warehouses, hangar bays, and obstructed areas, aqueous foams with very low water content are applied from foam generators located near the ceiling, quickly filling the space. In addition, aqueous foams with greater liquid content are sprayed on top of flammable liquids to suppress pool fires and build a foam bed above the pool to prevent re-ignition.

Another method of filling a container with foam is by introducing gas bubbles into a liquid solution containing surfactants. The gas bubbles rise to the surface of the liquid solution, forming a foam bed above the liquid. In this case, the fresh foam is added to the bottom of the column. Examples of applications employing this method include foam fractionation used by pharmaceutical and food industries for protein separation, and froth flotation used by the mining industry for mineral separation.

The loss of liquid from foam, also called foam drainage, has a crucial impact on its effectiveness in applications. The dominant force responsible for drainage is gravity, which acts on the foam from the moment it is generated. However, most drainage models describe the drainage of liquid from foam by starting with a stationary foam column of fixed height. This approach neglects the effect of gravity during an essential stage of foam applications, the filling process. Significant liquid loss could occur over the filling time, which would ultimately alter the effectiveness of the foam.

Modeling efforts aim to understand foam drainage by considering the flow of liquid through the foam. The liquid flow in foam depends on the geometry of the liquid contained in the interstitial space between foam bubbles. The foam bubbles take on shapes similar to polyhedra. In Figure 1, an illustration depicts a bubble shaped as a dodecahedron and the surrounding liquid structures: films, channels, and nodes. The films are thin sheets of liquid formed where the surfaces of two bubbles meet. The channels are formed at the intersection of three bubbles: channels are also called Plateau borders in honor of pioneer foam scientist J. A. F. Plateau. The cross section of a channel resembles a triangle with edges curved toward the interior. The channels can be considered as a network of pipes that allow liquid to flow through the foam. The junctions where the channels intersect are called nodes; and four channels meet at a single node. The dimensions of films, channels , and nodes depend on the bubble size and the liquid content of the foam. The amount of liquid contained in the foam can be quantified in terms of the foam expansion ratio $\left(Ex\right)$: the ratio of the foam volume to the volume of liquid

Manuscript approved November 8, 2010.

solution used to form the foam; or the liquid volume fraction (α) : the ratio of liquid volume to total foam volume (Note that $Ex = 1/\alpha$).

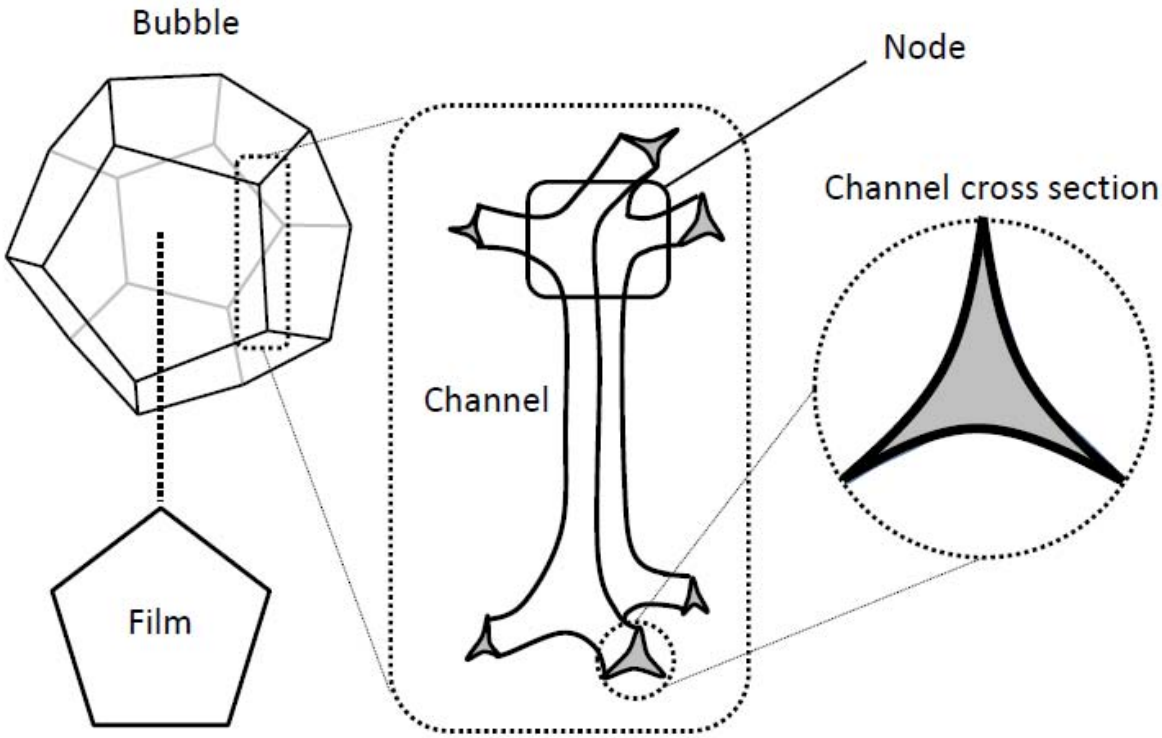

Figure 1: Illustration of films, channels, and nodes for an idealized dodecahedral bubble.

Most of the modeling and experiments on foam drainage have been performed on stationary foams with low expansion ratios. Leonard and Lemlich [1] modeled steady-state drainage from a foam fractionation column, where foam is continuously formed at the base of the column. The modeling approach, which is the basis for most models, involved a description of the liquid flow within the channels by considering forces due to gravity, variation in liquid (capillary) pressure along the height of the column, and viscous resistance to liquid flow. The latter varied with a parameter termed surface viscosity, which was used to quantify the mobility of the channel walls.

Desai and Kumar [2] examined the semi-steady-state liquid fraction as a function of height within a column under similar conditions, including the loss of liquid from the films with time. The model contained channels with a simplified cross section, an equilateral triangle. A parameter was introduced to account for the mobility of the channel walls [3]. The effects of viscosity, surface viscosity, and input gas flow rate on the steady-state liquid-fraction profile were examined with experiments using the surfactants sodium lauryl sulfate (SDS), lauryl alcohol, and Teepol. The average, steady-state Ex values ranged from about 10 to 100.

Ramani, Kumar, and Gandhi [4] proposed a model for drainage from a static foam column that accounted for the time-dependent drainage of films into nearly vertical and nearly horizontal Plateau borders, where gravity was a driving force only for the liquid contained in the nearly vertical channels. The model was compared with experiments using the surfactant SDS with $Ex \approx 8$ and bubble diameters less than $7 \times 10^{-4}\ m$. Podual, Kumar, and Gandhi [5] later changed the bubble geometry from dodecahedral to tetrakaidecahedral along with the channel orientation of the model, and the adjustments slightly improved the comparison with experiment for small bubble sizes. The experiments included foams with expansion ratios up to 100 and bubble diameters up to $7 \times 10^{-3}\ m$.

The model of Verbist [6] contained a foam drainage equation which included non-steady-state variation in the cross-sectional area of the foam channels, allowing the liquid fraction of the foam to change with both position and time. The ability to calculate a time-varying liquid fraction including the changing area of the channels allowed the model to study the free drainage problem: to describe drainage from a fixed-height column of foam with a liquid fraction that is initially uniform. The model viewed the foam channels as a set of independent vertical pipes with strictly immobile walls. As in most recent models of drainage, the contribution of the films was neglected. Channels were considered in the equations for the conservation of liquid volume and momentum of the model, where an effective viscosity (about 150 times that of water) was introduced to account for the cross-sectional geometry and random orientation of the channels.

The approach of Koehler [7] viewed foam drainage as the flow of liquid through a porous medium, such as a filter. From this perspective, the proportionality between the flow rate of liquid through the foam and the pressure gradient that drives the liquid flow is determined by a permeability function, which depends on the local liquid fraction. The model calculations were compared with experimental results using the surfactant SDS and gaseous C_2F_6 to minimize the diffusion of gas between bubbles. The expansion ratio studied for free drainage from a static foam column was 200 and the bubble diameter was approximately $4 \times 10^{-3}\ m$. The work suggests, in contrast to the model of Verbist, that the viscous effects could be predominantly acting in the nodes rather than the channels for foams with highly mobile walls.

Magrabi et al [8,9] investigated free drainage from AFFF and FFFP compressed-air foams used in fire suppression. The foams initially had an expansion ratio of 20 and a bubble diameter of approximately $2.6 \times 10^{-4}\ m$. The model contained a wall mobility parameter similar to that of Desai and Kumar [2,3]. The work suggests that an effect not included in the model, the increase in average bubble size caused by gaseous diffusion between bubbles, could significantly increase the drainage rate in these foams after a few minutes.

A few recent works have investigated forced and pulsed drainage. These processes involve the continuous and finite addition of liquid to the top of a foam, respectively. Drainage under these conditions has been studied by the non-steady-state models of Verbist [6] and Koehler [7]. In forced drainage, the liquid volume fraction becomes uniform behind a traveling

liquid front that moves through the foam at a constant velocity. As shown by the two studies [6,7], the front velocity displays different power-law dependence on the liquid fraction depending on the surfactant solution used. However, forced and pulsed drainage models do not apply to the case of filling a container with foam.

Bhakta and Ruckenstein [10] have investigated filling a container with foam from the bottom, as in the process of foam fractionation. To account for the filling process, the model included a single moving boundary, the foam front, and considered the non-steady-state behavior of the liquid content within the foam. The experimental data of Germick et al [11] that included bubble diameters of about 3×10^{-3} m to 4×10^{-3} m were used for comparison. In the study, the effect of foam fill rate on the drainage rate was not investigated.

In this work, we present theoretical analysis and experiments for drainage from a foam as it fills a container from above. We introduce to the drainage problem an additional time scale, the time required to fill the column with foam. This additional time scale changes the effect of drainage on the liquid fraction of the foam. Two moving boundaries are treated in the problem: the air/foam interface where foam is added at the top and the foam/liquid interface where the foam layer meets the drained liquid that collects beneath it. The height of the foam bed is therefore controlled by both the rate of foam injection and the rate of liquid drainage. We also treat free drainage as a special case of the model, wherein there is a single moving boundary at the foam/liquid interface.

We focus our investigation on one type of aqueous foam used *in practice* for fire suppression generated with a surfactant designed for achieving high expansion (HiEx). The foams possess greater expansion-ratio values and bubble sizes than those investigated in most previous works. An important aspect of this work is that we provide analytical solutions for the liquid drained from the foam and the average liquid fraction of the foam as functions of time. The analytical solutions offer the ability to quickly predict drainage and to clearly understand how the various parameters influence the behavior. Similar to previous works, the model contains an adjustable parameter called a permeability coefficient that accounts for the geometry of the channels as well as the mobility of the channel walls. The solutions allow the permeability coefficient for a given foam to be calculated by fitting to experimental data. We show good agreement with experimental results by treating the permeability coefficient as a constant. We use the model to examine the effect of fill rate, expansion ratio, column height, and bubble size on the drainage behavior.

2.0 MODEL

Filling a container from above involves delivering fresh foam to the top of a growing foam bed, and the injection of foam is ceased when the container is full. Both during and after the filling period, liquid drains out of the foam and forms a liquid layer beneath the foam bed. During the process of drainage, bubble films empty a portion of their liquid to the surrounding channels. Liquid in the channels moves downward, passing through nodes into lower channels repeatedly as it makes its way out of the bottom of the foam. As the liquid content of the foam

diminishes, the films reduce in thickness, the nodes shrink in volume, and the cross-sectional area of the channels decreases.

There are several physical factors that drive the flow of liquid in foam. For the foams of interest, the forces governing fluid transport within the foam are not in an equilibrium state when the foam is generated. For foam with sufficient liquid content, the gravitational force is initially dominant for the liquid in the channels and nodes, driving liquid downward within the foam. Liquid flow can also be driven in a foam when there is a spatial variation in *capillary pressure*, the pressure difference between the liquid and gas at the curved surface of a bubble. The capillary pressure is caused by the surface tension at the interface of the two phases, gas and liquid, within the foam which acts to minimize the surface area of the interface.

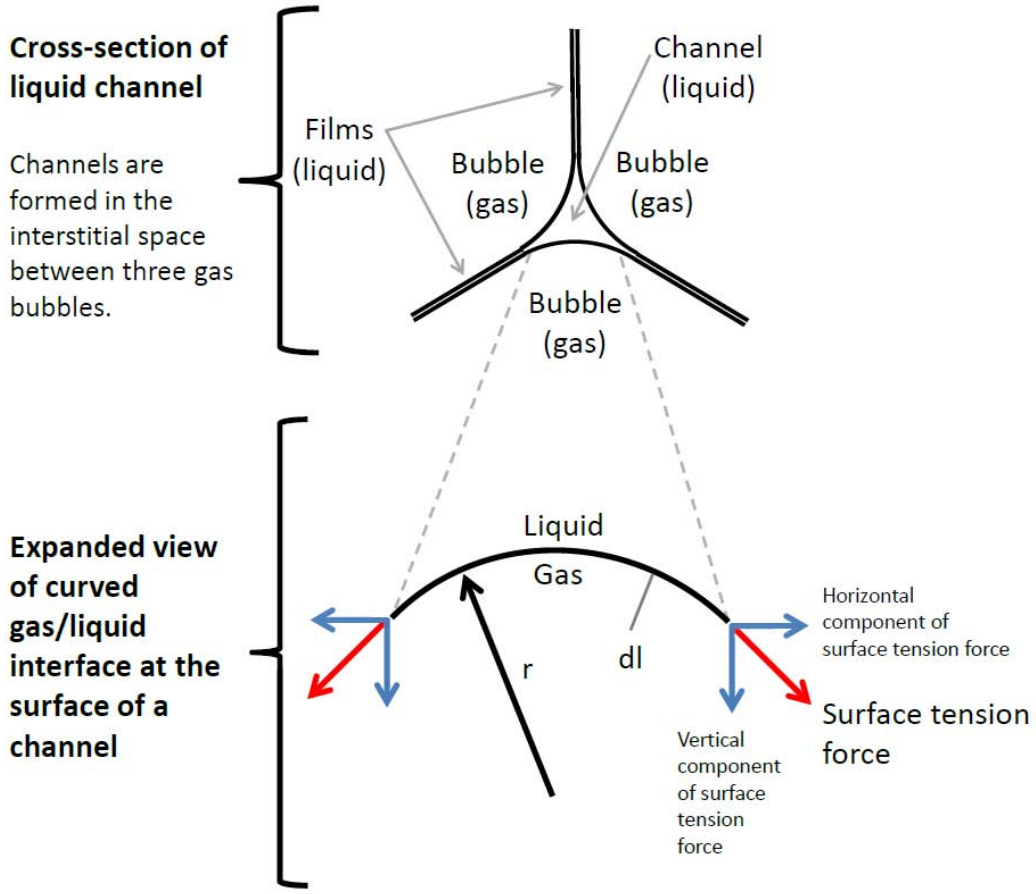

Figure 2: Surface tension force at the gas/liquid interface of a bubble.

To see how surface tension gives rise to capillary pressure in a foam, consider the illustration of the curved gas/liquid interface at the surface of a channel in Figure 2. The surface tension force is directed along the surface and pulls at each end of a surface length element dl. The horizontal components of the surface tension acting on a surface length element dl

cancel, but the vertical components do not. The net force on each curved interface is directed toward the adjacent gas bubble and its magnitude is inversely proportional to the radius of curvature of the surface. The surface tension force therefore increases the pressure of the gas relative to the surrounding liquid by compressing the bubbles at the curved surfaces of the channels. The Young-Laplace law

$$P_g - P_l = \frac{\gamma}{r} \tag{1}$$

provides a relation between the gas pressure, P_g, and the liquid pressure, P_l, that is valid at the gas/liquid interface. Note that the pressure of the liquid in the films approaches the pressure of the surrounding gas bubbles because the films are very flat, i.e. r is very large.

The curvature at the surface of channels can vary throughout different regions in a foam. Channels with more liquid have a larger radius of curvature, and therefore have a smaller capillary pressure, i.e. the liquid pressure gets closer to the gas pressure. In a draining column of foam, the liquid content at the top of the foam becomes smaller than that of the bottom. Hence, a gradient in the capillary pressure is established, which drives the flow of liquid. For a draining column, the flow due to the gradient in capillary pressure opposes the gravitational flow.

Additionally, the flow of liquid through a foam depends on the degree of slip at the channel boundaries. Slip is a term used to describe the flow of liquid relative to its bounding surface; a no-slip condition in a channel means that the liquid velocity at the channel walls is zero. Slow or non-moving liquid at the walls causes a variation in liquid velocity (i.e. stress) across the channel cross section, giving rise to viscous drag that impedes flow within the channel. The slip condition depends on the mobility of the gas/liquid interface at the surface of the bubbles. If the surface of the channel is able to freely move along with the flowing liquid, it would cause plug flow, a uniform liquid velocity profile across the channel cross section. The slip condition for foam channel flow lies within these extrema and can result in different drainage rates for the foam as a whole. Evidence suggests that the mobility of the surface and hence the slip condition strongly depends on the surfactant. In fact, studies have shown that the drainage rate from a foam can be significantly reduced by adding a different surfactant [12].

A suggestion for the physical origin of the mobility of the channel walls is that the liquid flowing nearby could shear surfactant molecules from the gas/liquid surface [7]. If the shearing creates a concentration gradient on the surface, then diffusion of surfactant on the surface could oppose liquid flow. However, if the surfactant in the flowing liquid can move to the surface much faster than the rate of shear, then the surfactant can quickly replenish the surface without establishing an appreciable concentration gradient. An alternative argument involves the idea of viscosity at the surface, which reflects the forces of attraction between surfactant molecules. The strength of the interaction could also be so large that the channel flow is not strong enough to shear the molecules apart. If one considers the films as stationary, then the channel walls would be immobile because they are “anchored” to the films. Weaker interactions may allow the surfaces to shear.

Further, in a polydisperse foam, bubbles of different sizes differ in their gas pressure. Small bubbles exhibit greater pressure and Henry's law states that the solubility of gas in the surrounding liquid will be greater. Neighboring bubbles with lower pressure will have surrounding liquid with lower gas solubility. Hence, a concentration gradient of dissolved gas is established in the liquid phase, driving the dissolved gas toward the larger bubble(s). This process is called Ostwald ripening and it makes an appreciable contribution to *coarsening*, the process of increasing foam average bubble size over time. The time scale associated with coarsening can vary significantly between foams [13]; the study of Magrabi [8] on AFFF foams formed with compressed air shows that bubble size begins to increase within just a few minutes. Another factor that contributes to coarsening is *coalescence*, where film rupture between two bubbles produces a single, larger bubble.

In our model, we set up the problem such that the foam is injected at a constant velocity. Further, we consider one-dimensional drainage along the z-direction as depicted in Figure 3. The drainage problem is reduced to a single dimension because the forces that dominate liquid transport are in the vertical direction until the foam approaches equilibrium.

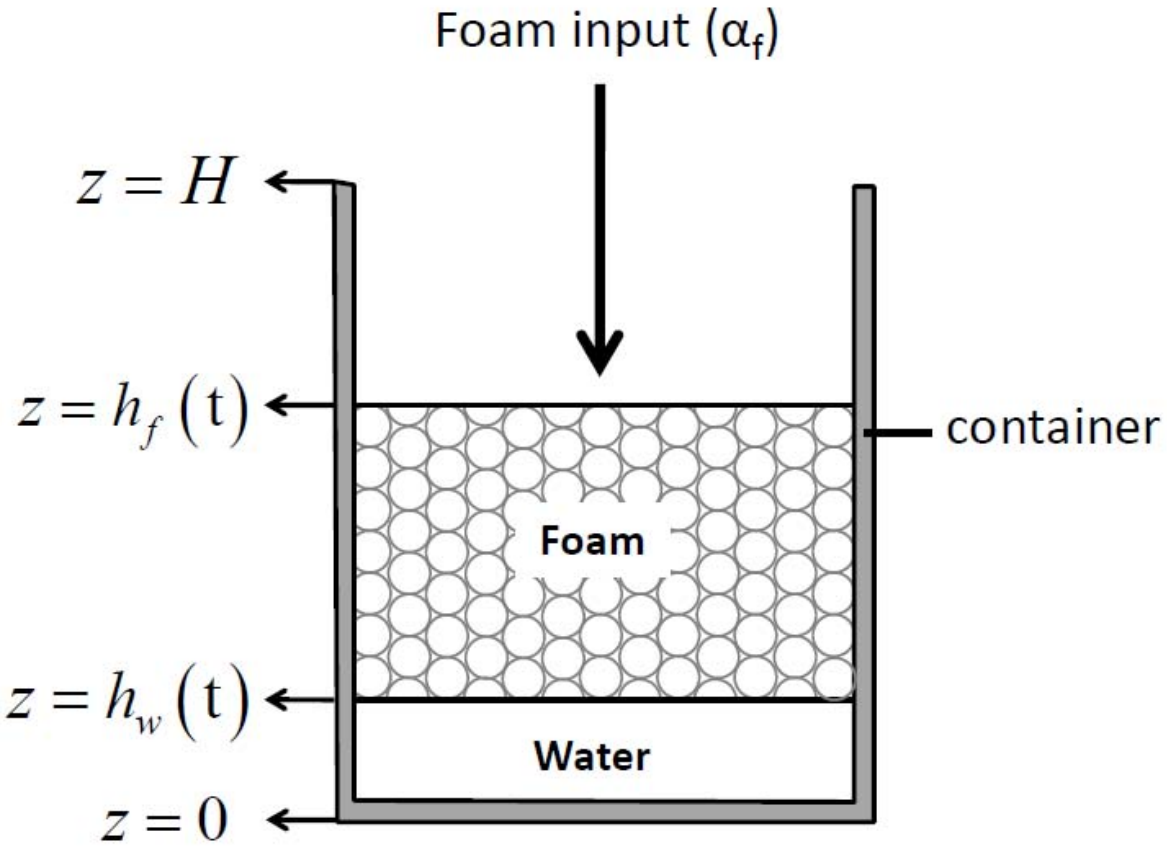

Figure 3: Illustration of drainage model including moving boundaries.

We consider two moving boundaries. The first boundary, $z = h_f(t)$, is the air/foam interface that moves towards the top of the foam column at the injection velocity v_{inj}, defined as the foam injection rate per unit cross-sectional area of the container. The second boundary, $z = h_w(t)$, is the foam/liquid interface, where the solution drained from the foam pools beneath it. The volume of liquid drained is $V_d = Sh_w(t)$, where S is the cross-sectional area of the foam column. Once foam injection stops, the top of the foam layer is fixed at the height of the column, H, and the foam/liquid interface is the only moving boundary. This situation corresponds to free drainage of a foam on top of liquid.

Our goal for the model is to predict the amount of water drained from a foam and the change in the foam expansion ratio over time in bench-scale experiments. Hence, for both filling drainage and free drainage, the model solves for the height of the moving foam/liquid interface, $h_w(t)$, and the liquid fraction of the foam averaged over the length of the foam layer, $\bar{\alpha}(t)$.

Approximations are made in the model for the foam structure. We neglect the drainage of liquid from the thin films, and we therefore only consider the channels. For large bubbles, the portion of liquid in the films is negligible [14]. Further, the shape of bubbles in this work has been approximated as dodecahedral, where the channels are formed at the bubble edges. Although the shape leaves a small amount of space unaccounted for, the work of Podual *et al.* [5] indicates that the difference between tetrakaidecahedral and dodecahedral geometries in drainage models is negligible for large bubbles. Also, we consider a monodisperse foam, where each gas bubble has the same volume. In practice, foams contain a distribution of bubble sizes. Similar to the approach of Magrabi *et al.* [8], we assume that the drainage behavior of a polydisperse foam can be captured by modeling the foam as monodisperse, with a bubble size equal to the average of the bubble-size distribution.

We maintain a constant bubble size in the model and therefore neglect the effects of both Ostwald ripening and coalescence. For Ostwald ripening to occur, there must be a pressure difference between bubbles that yields a concentration gradient in the dissolved gas. For larger bubbles, the radii of curvature within the foam will be larger, causing a decrease in the capillary pressure. If the dispersity in the bubble-size distribution is not large, then the pressure differences between bubbles should be small. Hence, it is likely that the phenomenon that drives Ostwald ripening should be less important for large bubbles. By the reasoning above, the gas pressure is treated as a constant in the model. The liquid pressure in the channels is assumed equal to the pressure of the liquid at the bubble/channel interface, given by the Laplace-Young law.

As for coalescence in the model, recent work [13] shows that the onset of coalescence depends primarily on a critical liquid fraction and is independent of bubble size. The surfactants investigated in Ref. [13] were TTAB and SDBS; each foam studied exhibited a critical liquid fraction less than 0.0008 $(Ex = 1250)$. The calculations of our model indicate that this liquid

fraction is approached only near the end of the time for which we are interested in simulating the drainage process. Assuming that the foams in our study have a similar critical liquid fraction for the onset of coalescence, the effect of coalescence should be negligible in our study during the drainage period of interest.

The mobility of the channel walls is not explicitly accounted for in the model. We have included an adjustable parameter, the permeability coefficient, which accounts for the mobility of the channel walls, random orientation of the channels, and corrections to the geometrical approximations of the model. Note that most drainage models include either an adjustable parameter for wall mobility or assume that the channel walls are immobile.

From the partial differential equations (PDEs) governing mass and momentum balance of the liquid in a foam, we seek ordinary differential equations (ODEs) with time as the independent variable to arrive at analytical solutions that describe the drainage process. By approximation, we solve for the height of the water layer beneath the foam, h_w, and the length-averaged liquid fraction of the foam, $\bar{\alpha}$. A detailed description of the solution is provided below.

We develop the model by considering the partial differential equations for mass and momentum balance in one dimension. Treating the liquid as incompressible, the liquid volume balance in the foam is given by

$$\frac{\partial \alpha}{\partial t} + \frac{\partial}{\partial z}(\alpha v) = 0 \tag{2}$$

where $\alpha = \alpha(z,t)$ is the liquid fraction of the foam and $v = v(z,t)$ is the liquid velocity. The liquid velocity of the model, discussed below, is an effective vertical velocity of the liquid averaged over the cross-sectional area of a channel. The superficial liquid velocity is $v_s = \alpha v$, which is the volume of liquid flowing through a unit of cross-sectional area of the foam column per unit time. As illustrated in Figure 5, the liquid in the channels travels through the channel cross section at velocity v, whereas the liquid exiting the foam (or a control volume) travels through the foam-column cross section with the velocity v_s. The balance in (2) is written for a control volume of the foam; for the column considered, the control volume corresponds to a disc with the same cross-sectional area of the foam column, but with a small thickness. The previous expression states that if the superficial velocity of the liquid coming into the control volume is different from the output superficial velocity, there is a corresponding change in the liquid fraction within the control volume.

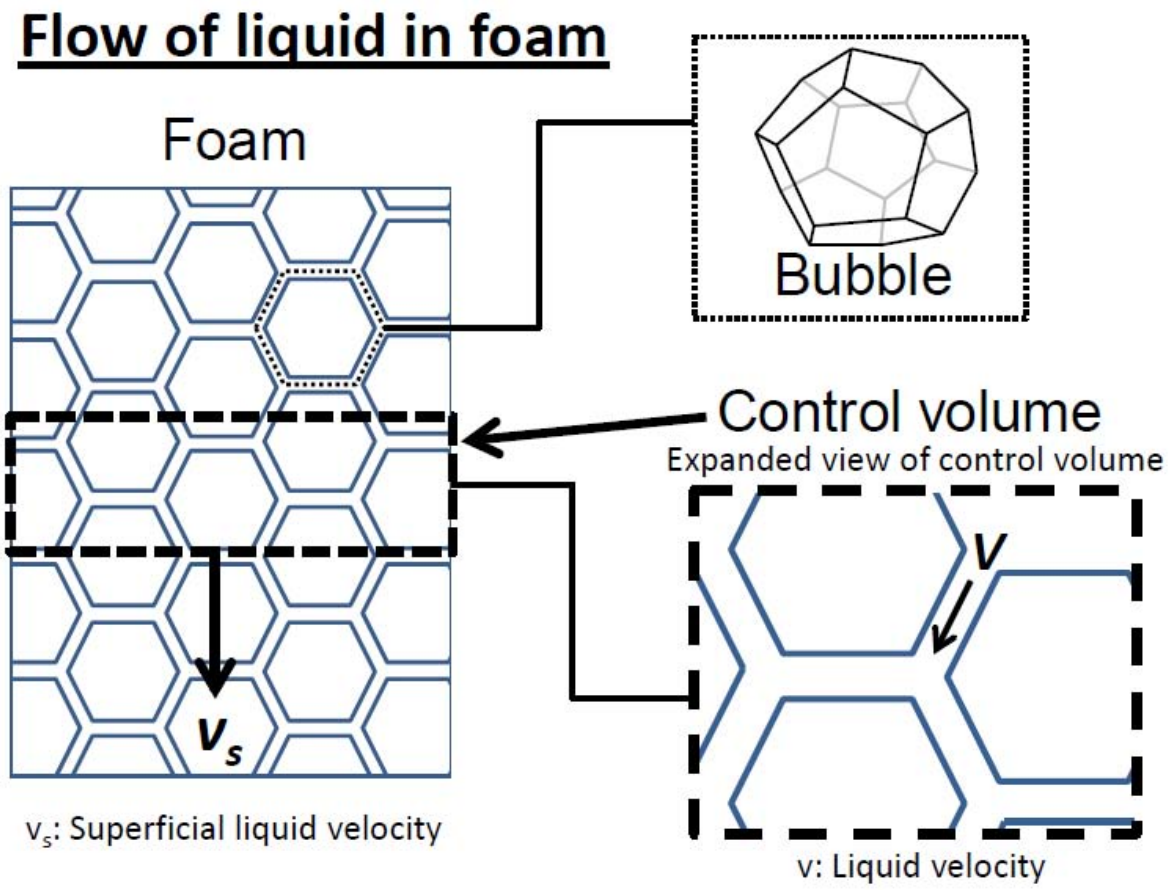

Figure 4: Illustration of the flow of liquid within the foam.

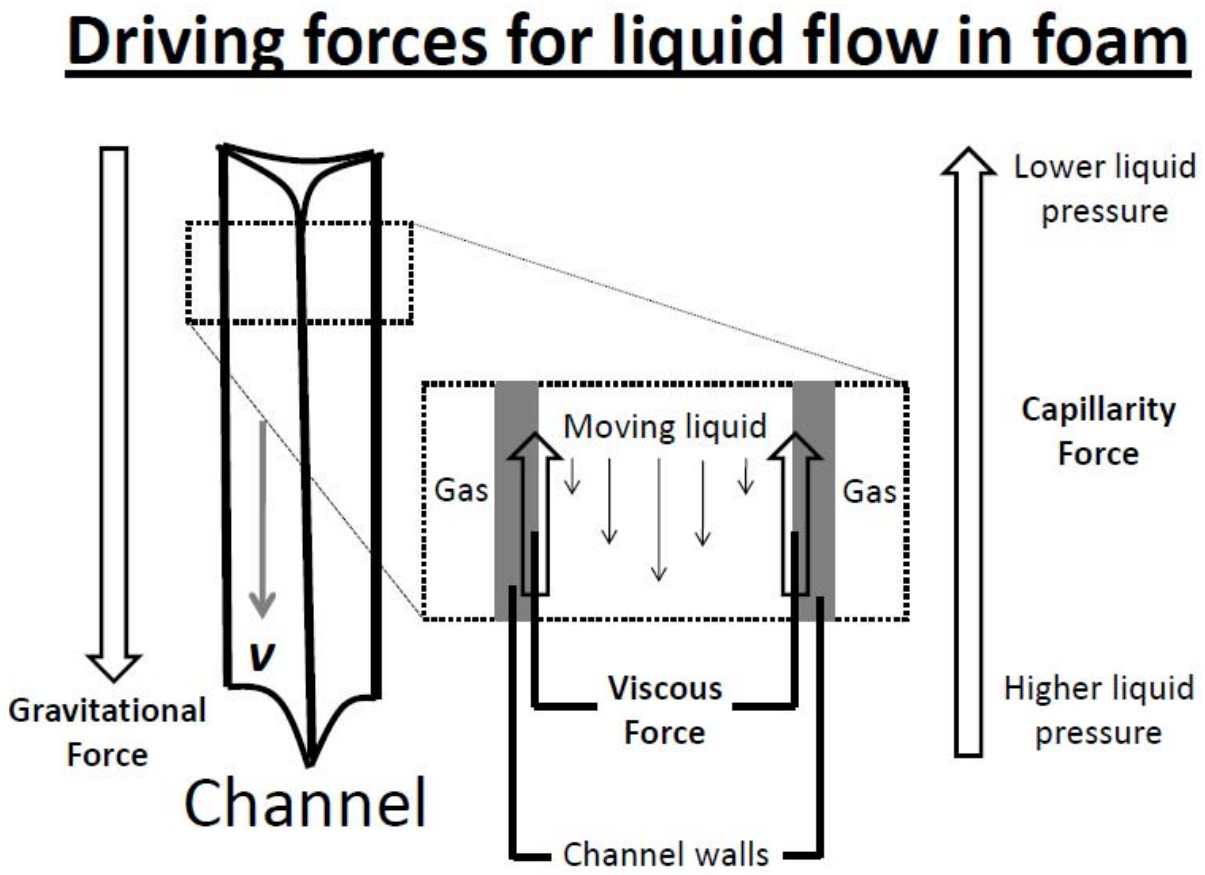

Figure 5: Illustration of the forces that drive the flow of liquid in foam.

Next, we consider some of the geometrical approximations of the model that will be necessary for the momentum conservation equation. The bubble shape in the model is a regular pentagonal dodecahedron, and this is used to relate the geometrical parameters of the bubble and its corresponding channels to the local liquid fraction of the foam. There are n_p channels per bubble; for a dodecahedral bubble, the number of channels is equivalent to the number of edges that belong to a single dodecahedron, $n_p = 10$. Each channel has length L and area a_p, and the liquid volume contained in the channels per bubble is therefore $n_p a_p L$. We neglect the additional volume of liquid contained in the nodes, which should be very small for the high-expansion foams of interest. The volume of gas contained in a dodecahedral bubble is $V_b = GL^3$, where $G = (15+7\sqrt{5})/4 \approx 7.66$, and the total volume of gas and liquid per bubble is the sum of these quantities.

We view the foam column as a space filled by a collection of bubbles and their respective channels, where the liquid fraction of an individual bubble unit is equivalent to the liquid fraction of the foam as a whole. We therefore get the expression

$$\frac{n_p a_p L}{n_p a_p L + V_b} = \alpha \quad \Rightarrow \quad \frac{n_p a_p L}{V_b} = \frac{\alpha}{1-\alpha}. \tag{3}$$

For a high expansion ratio, $\alpha << 1$, and we therefore make the approximation

$$\frac{n_p a_p L}{V_b} = \alpha. \tag{4}$$

The cross-sectional area of the channel is related to the radius of curvature by $a_p = \delta_a r^2$, where $\delta_a = \sqrt{3} - \pi/2 \approx 0.161$. By substituting this relation and $V_b = GL^3$ into (4), we have a relation between the liquid fraction of the foam and geometrical parameters of the bubbles:

$$\alpha = \frac{n_p \delta_a r^2 L}{GL^3} = \delta \left[\frac{r}{L}\right]^2 \tag{5}$$

where $\delta \approx 0.21$. This approximation was made by Koehler [7] for tetrakaidecahedral bubbles. Note that the relationship between cross-sectional area of the channel and local liquid fraction is

$$a_p = \frac{G}{n_p} \alpha L^2. \tag{6}$$

To understand the dependence of the channel area in (6), consider the liquid and gas content of a single bubble. If the volume of the gas bubble remains constant, increasing the liquid fraction of the bubble by adding liquid to the channels will cause the channels to swell, increasing the channel cross-sectional area. Also, for a bubble that, regardless of size, maintains a constant liquid fraction, the channel volume is proportional to $a_p L$ but the total volume of the bubble is proportional to L^3. The liquid volume fraction is therefore proportional to a_p / L^2. For the liquid fraction to be constant as the bubble size increases, a_p must also be proportional to L^2. Hence, the channel cross-sectional area depends on both the liquid fraction of the bubble and the square of the channel length.

Next, we seek an expression for the momentum balance for a channel that is oriented vertically within the foam. For a given liquid and pressure gradient across a channel, the velocity of flow through a channel will depend on the channel geometry and the slip condition at the channel walls. Deriving an expression for the average liquid velocity in a channel is complicated because the cross-section of the channels has a complex shape and we do not predict or measure the slip condition. Given the difficulty of the problem, we aim to show, under simpler conditions, that the average velocity should be proportional to the channel area. In Appendix A, we derive an equation for the average velocity through a cylindrical channel with a circular cross section and a no-slip condition at the boundary. The result is quoted here:

$$v = \left[\left(\frac{\left(15+7\sqrt{5}\right)}{320\pi\mu}\right)\alpha L^2\right]\left(\rho\mathbf{g} - \frac{\nabla(\alpha P_l)}{\alpha}\right) = \left[\left(\frac{1}{8\pi\mu}\right)a_p\right]\left(\rho\mathbf{g} - \frac{\nabla(\alpha P_l)}{\alpha}\right) \quad . \tag{7}$$

The velocity in (7) is very similar to the well-known Hagen-Poiseuille equation for flow in a cylindrical pipe.

The same dependence of v on a_p is shown in the expression derived by Desai and Kumar [2] for general wall mobility in channels with the cross-section of an equilateral triangle

$$v = \frac{c_v a_p}{20\mu\sqrt{3}}\left(\rho g - \frac{\partial P_l}{\partial z}\right) = \frac{c_v\left(15+7\sqrt{5}\right)\alpha L^2}{800\mu\sqrt{3}}\left(\rho g - \frac{\partial P_l}{\partial z}\right) \quad . \tag{8}$$

The parameter c_v is a velocity coefficient defined as the ratio of the average velocity in a channel to the velocity of the same channel if the walls are strictly immobile.

In both cases, the average velocity in the channel can be described by

$$v = \frac{\xi\alpha L^2}{\mu}\left(\rho g - \frac{\partial P_l}{\partial z}\right) \tag{9}$$

where ξ, defined here as a permeability coefficient, accounts for bubble and channel geometry, slip condition, and the orientation of the channels. In this work, ξ is an adjustable parameter of the model.

We reiterate that the pressure in the liquid is found from the Young-LaPlace law,

$$P_l = P_g - \frac{\gamma}{r} \tag{10}$$

which, at a gas-liquid interface with surface tension γ, relates the pressure of the gas in the bubbles, P_g, to the pressure of the surrounding liquid in the channel with radius of curvature, r.

The pressure gradient $\partial P_l / \partial z$ is found by substitution of (5) into (10),

$$\frac{\partial P_l}{\partial z} = \frac{\partial}{\partial z}\left[P_g - \frac{\gamma\sqrt{\delta}}{L\sqrt{\alpha}}\right] = -\frac{\gamma\sqrt{\delta}}{L}\frac{\partial}{\partial z}\left[\frac{1}{\sqrt{\alpha}}\right]. \tag{11}$$

An expression for the average velocity in a channel as a function of the liquid fraction then becomes

$$v = \frac{\xi \alpha L^2}{\mu}\left[\rho g + \frac{\gamma\sqrt{\delta}}{L}\frac{\partial}{\partial z}\left[\frac{1}{\sqrt{\alpha}}\right]\right]. \tag{12}$$

Note that, overall, the velocity is proportional to the area of the channel, which is also proportional to αL^2. Meanwhile, the pressure gradient involves the gradient of $1/r$ where the radius of curvature $r \propto \sqrt{a_p} \propto L\sqrt{\alpha}$. The combined liquid-fraction dependence in the pressure gradient term should therefore involve the gradient of the radius of curvature (i.e. $\sqrt{\alpha}$). This is shown by the simplification

$$\alpha\frac{\partial}{\partial z}\left[\frac{1}{\sqrt{\alpha}}\right] = -\frac{\partial}{\partial z}\left[\sqrt{\alpha}\right] \tag{13}$$

Substitution of the previous expression in (12) yields an equation for the average liquid velocity in a channel

$$v = A\alpha - B\frac{\partial}{\partial z}\left(\sqrt{\alpha}\right), \tag{14}$$

where we introduce the constants

$$A = \left(\frac{\xi L^2 \rho g}{\mu}\right) \tag{15}$$

and

$$B = \left(\frac{\xi L \gamma\sqrt{\delta}}{\mu}\right). \tag{16}$$

The units for A are m/s (velocity) and for B are m^2/s (area/time).

For a given foam, (14) indicates that the average liquid velocity in a channel is determined by a dynamic competition between the liquid fraction and its variation along the height of the column. Equivalently, this is a competition between the local channel area and the vertical gradient in the radius of curvature. For regions of foam with uniform liquid fraction, the average velocity is proportional to the corresponding liquid fraction. For cases wherein a foam is filled very fast such that the liquid fraction is approximately equal to the input, one should expect a constant superficial velocity $v_s \approx A\alpha_f^2$. For slower filling, the liquid fraction will vary along the height of the column, decreasing at the top and increasing near the foam/liquid interface. For this case, the effects combine in different regions. At the end of filling, the liquid fraction will quickly decrease with column height; the dynamic effects of the liquid fraction and its gradient will oppose one another throughout the height of the foam. Drainage ceases at equilibrium when these terms are equal in magnitude.

The average liquid velocity in a channel also depends on multiple parameters. For any case, it is proportional to the permeability coefficient and inversely proportional to the viscosity of the liquid. By definition, a greater permeability coefficient increases the velocity of the liquid in the channels. The viscosity plays a role because we are considering the case where the liquid at the walls is moving slower than the rest of the liquid in the channel. A more viscous liquid will reduce the velocity difference between neighboring liquid "particles", and therefore reduce the average velocity within the channel, overall. For a given liquid-fraction profile, other parameters affect the strength of the terms in (14) on the competition that determines the velocity. The constant A is proportional to L^2, reflecting that the term is proportional to the channel area $a_p \propto \alpha L^2$. Further, the effect of gravity is contained in A, which always acts to increase the liquid velocity flowing in a vertical channel. The value of B determines the strength of the effect of liquid fraction variation with height on average channel velocity. In contrast with A, B increases linearly with channel length L, which indicates that A will be dominant for larger bubbles sizes. An essential parameter in B is the surface tension, γ, which is responsible both for the existence and strength of the capillarity effect for a given variation in the liquid fraction with height.

Boundary conditions must be imposed on α. We treat the case for which α is constant at the boundaries. During filling, the top of the foam contains the liquid fraction of the fresh input foam, α_f. The choice for the liquid fraction at the foam/liquid boundary is less obvious. Similar to the approach of Desai and Kumar [3], we assume that the bubbles are close-packed in a face-centered cubic (fcc) arrangement. Further, the shape of the bubbles is approximated as spherical, and the liquid fraction at this boundary is assumed equal to the void fraction of close-packed spheres in an fcc arrangement, $\alpha(z = h_w) = 0.26$. The boundary conditions are also used during free drainage for comparison with the experiments of this work. After filling, the liquid volume fraction at the top of the foam significantly decreases from α_f. However, we find that reducing the value of the liquid fraction at the top boundary below α_f has a negligible effect on the predictions of the model. We maintain the same boundary conditions for filling and free drainage to avoid unnecessary complication of the model parameters.

The drainage model in this work is similar to other drainage models in the literature [6-10], and the equations governing the conservation of mass and momentum within the foam can be expressed in the same form. The general form is:

$$\frac{\partial \alpha}{\partial t} + \frac{\partial}{\partial z}(\alpha v) = 0 \qquad v = \frac{\xi}{\mu}\left(\left[\rho g L^2\right]\alpha - \left[\gamma L \theta\right]\frac{\partial}{\partial z}\left(\sqrt{\alpha}\right)\right) \quad , \tag{17}$$

where $\theta = 0.46$ except as noted below. The values of the permeability coefficient ξ from the literature and from this work are provided in Table 1. The large values used to model the experiments of Magrabi et al. [8,9] indicate that the foams in their study drain much faster than the foams studied in the other works listed, which is assumed to be a result of channel wall mobility. The other calculated and empirical values for ξ are for foams with immobile channel walls. For randomly oriented channels, the reported values for ξ are smaller and vary at most

by about 20%.; the largest contribution to the difference between these values is the bubble geometry of the model. In this work, we also calculate ξ for vertically oriented channels with no slip at the channel walls, which is the largest physically reasonable value of ξ for this slip condition.

Table 1: Permeability coefficients of foam drainage models.

Work	Calculation method	ξ	Surfactant (type)
Bhakta and Ruckenstein (Ref. [10])*	Calculated for randomly oriented channels with triangular cross section and immobile walls[D]	0.0055	Model results compared with experimental data of Ref. [11] using Bovine Serum Albumin, BSA (protein)
Koehler et al. (Ref. [7]) †	Calculated for randomly oriented channels with scalloped-triangular cross section and immobile channel walls[T]	0.0063	N/A
Magrabi et al. (Ref. [8])*	Empirically determined from drainage theory for randomly oriented channels with triangular cross section and mobile walls[D]	0.0245‡	Aqueous film-forming foam, AFFF: contains perfluoroalkyl sulfonate salts (fluorocarbon based)
Magrabi et al. (Ref. [9])*	Empirically determined from drainage theory for randomly oriented channels with triangular cross section and mobile walls[D]	0.0105‡	Film-forming fluoroprotein foam, FFFP: contains hydrolized proteins and fluorosurfactants (fluoroprotein)
Verbist et al. (Ref. [6])◊	Calculated for randomly oriented channels with scalloped-triangular cross section and immobile walls	0.0051	N/A
This work	Empirically determined from drainage theory for randomly oriented channels with scalloped-triangular cross section and immobile walls (Ref. [7])[D]	0.0051	Buckeye HXF 2.2% High-Expansion Foam Concentrate: contains sodium laureth sulfate (hydrocarbon based)
This work	Calculated for vertically oriented cylindrical and equilateral triangular channels with immobile walls (see Appendix A)[D]	Cylindrical: 0.03 Triangular: 0.022	N/A

*Mathematical form of Eq. (17) obtained when α <<1

† $\theta = 0.41$

‡ ξ for initial liquid volume fraction 0.05

◊Equation (6) of this work used to relate a_p to α

[D]Assumed dodecahedral bubble geometry, L=0.816R

[T]Assumed tetrakaidecahedral bubble geometry, L=0.72R

The next step in the development of the model is to obtain ordinary differential equations from the partial differential equations that describe the balance of liquid volume and momentum in the foam. To eliminate the spatial dependence of the equation for liquid volume balance, we integrate (2) with respect to the vertical coordinate z from the height of the liquid beneath the foam , h_w, to the height at the top of the foam, h_f:

$$\int_{h_w}^{h_f} \frac{\partial \alpha}{\partial t}\, dz + \alpha(h_f,t)v(h_f,t) - \alpha(h_w,t)v(h_w,t) = 0\,. \tag{18}$$

Using Leibniz's rule and the boundary conditions $v(h_f,t) = v(h_w,t) = 0$, this expression yields

$$\frac{d}{dt}\int_{h_w}^{h_f} \alpha\, dz - \alpha\left(h_f,t\right)\frac{dh_f}{dt} + \alpha\left(h_w,t\right)\frac{dh_w}{dt} = 0\,. \tag{19}$$

Let us define $\bar{\alpha}$ by the expression

$$\bar{\alpha} = \frac{\int_{h_w}^{h_f} \alpha(z,t)\; dz}{\left(h_f - h_w\right)} \tag{20}$$

where $\bar{\alpha}$ represents the length-averaged liquid volume fraction. The quantity $\bar{\alpha}$ is useful for providing an overall description of the liquid quantity in the foam. Substitution of (20) into (19) yields

$$\frac{d}{dt}\left[\bar{\alpha}\left(h_f - h_w\right)\right] = \alpha\left(h_f,t\right)\frac{dh_f}{dt} - \alpha\left(h_w,t\right)\frac{dh_w}{dt} \tag{21}$$

where $\alpha(h_f,t)$ is the liquid fraction at the top of the foam and $\alpha(h_w,t)$ is the liquid fraction at the bottom. For the present model, the liquid fractions at the boundaries will be considered as constants: $\alpha_f = \alpha(h_f,t)$ and $\alpha_w = \alpha(h_w,t)$. We consider that liquid drains from the foam into a liquid layer beneath the foam, and therefore we set $\alpha_w = 1$ for the liquid volume balance. The left-hand side of Eq. (21) is the time derivative of the liquid content within the foam, which is controlled by the quantities on the right-hand side. If we consider free drainage only, $dh_f / dt = 0$ and the rate of water loss can be determined by the rise of the water layer beneath the foam. However, by considering the case of filling, $dh_f / dt \neq 0$, the liquid content in the foam is now determined by the competition between filling and drainage. This competition can be controlled by the time scale introduced in the model, the fill time.

Integrating the momentum equation (14), we obtain

$$\int_{h_w}^{h_f} v\, dz = A\int_{h_w}^{h_f} \alpha\, dz - B\left(\sqrt{\alpha_f} - \sqrt{\alpha_w}\right). \tag{22}$$

We define the liquid velocity averaged over the height of the foam layer, $\overline{v}$, with the following expression

$$\overline{v} = \frac{\int_{h_w}^{h_f} v\, dz}{\left(h_f - h_w\right)}\ . \tag{23}$$

Inserting definitions (20) and (23) into (22) gives the expression

$$\overline{v}\left(h_f - h_w\right) = A\overline{\alpha}\left(h_f - h_w\right) - B\left(\sqrt{\alpha_w} - \sqrt{\alpha_f}\right). \tag{24}$$

Note that the boundary condition for α_w in the momentum balance is not the same as that for the liquid volume balance. The next step is to use these length-averaged quantities to determine an expression for the height of the water layer as a function of time, $h_w(t)$. The time derivative of h_w is the volumetric flow rate of liquid from the foam layer into the liquid layer per unit area of the foam column. Equivalently, this is the superficial liquid velocity exiting the foam,

$$\frac{dh_w}{dt} = v_s\,. \tag{25}$$

The liquid velocity and the superficial liquid velocity, both space- and time-dependent, are related by $v_s = \alpha v$. If the foam bed were separated into control volumes along the height of the column, the superficial velocity of the liquid exiting the foam due to drainage would be determined by the liquid balance of the control volume at the bottom of the foam near the foam/liquid interface. The superficial velocity of the liquid entering this control volume will depend on the balance over the control volume above, and the same is true for each control volume in the foam. Our approach does not resolve the foam column into control volumes; instead, we seek a description of foam drainage based on the average properties of the foam. We therefore make the approximation on the superficial velocity

$$\frac{dh_w}{dt} = \overline{\alpha}\,\overline{v} \tag{26}$$

and we assume that the error introduced in averaging is small. Solving for $\overline{v}$ in (24) and substituting in the previous expression yields an equation for the rate at which the height of the water layer increases

$$\frac{dh_w}{dt} = A\overline{\alpha}^2 - \frac{B\overline{\alpha}}{\left[h_f - h_w\right]}\left[\sqrt{\alpha_w} - \sqrt{\alpha_f}\right] \tag{27}$$

The expression above is used for both filling and free drainage conditions.

There are two ordinary differential equations in the model calculations, one for liquid volume balance, Eq. (21), and one for momentum balance, Eq. (27), where h_w and $\bar{\alpha}$ are unknown. In the following sections, two cases are considered for the model: the general case of filling and the special case of free drainage. For each, ordinary differential equations are presented that can be solved numerically. Additionally, approximations are made to obtain analytical solutions, and the conditions for which they are valid are discussed.

FILLING

For filling, we integrate Eq. (21) with respect to time to obtain the expression

$$\bar{\alpha}(h_f - h_w) = \alpha_f h_f - h_w + C_1 \tag{28}$$

where the last term is an integration constant representing the initial conditions,

$$C_1 = \bar{\alpha}(t_0)(h_{f0} - h_{w0}) - \alpha_f h_{f0} + h_{w0}\,. \tag{29}$$

The initial height of the water layer is set such that $h_{w0} = 0$. To prevent a singularity in Eq. (27), the problem is set up at $t = 0$ such that there is a small amount of foam with height $h_{f0} = 0.01\,m$ having the same liquid fraction $\bar{\alpha}(t_0) = \alpha_f$ as the foam that will fill the column. By setting this condition, we sacrifice the description of drainage behavior within the first few seconds of foam application, but this is not of interest for this study. Under these initial conditions, $C_1 = 0$. The liquid balance in (28) states that the liquid content in the foam is equal to the difference between the amount of liquid added to the foam and the amount of liquid that has drained out.

Solving for $\bar{\alpha}$ in (28) yields

$$\bar{\alpha} = \frac{\alpha_f h_f - h_w}{h_f - h_w}. \tag{30}$$

Substitution of this expression in Eq. (27) provides the filling equation

$$\frac{dh_w}{dt} = A\left[\frac{\alpha_f h_f - h_w}{h_f - h_w}\right]^2 - B\left[\frac{\alpha_f h_f - h_w}{\left[h_f - h_w\right]^2}\right]\left[\sqrt{\alpha_w} - \sqrt{\alpha_f}\right] \tag{31}$$

The previous expression is used for the numerical solutions during filling in this work. We also provide an analytical solution below. The numerical solutions were determined by the function NDSolve (MATHEMATICA, Wolfram Research) with default settings. NDSolve utilizes a variant of the Livermore Solver for Ordinary Differential Equations, LSODA, to numerically solve ordinary differential equations. Both stiff and non-stiff systems can be detected and solved

using LSODA, where backwards differentiation formula (BDF) methods and Adams methods are used, respectively.

Approximations are necessary in order to obtain an analytical solution for filling. First, we perform a Taylor expansion of $\bar{\alpha}^2$ about the value α_f

$$\bar{\alpha}^2 \approx \alpha_f^2 + 2\alpha_f \left[\bar{\alpha} - \alpha_f \right] = 2\alpha_f \bar{\alpha} - \alpha_f^2 \tag{32}$$

The value of $\bar{\alpha}^2$ must be greater than zero, so the approximation clearly fails if the condition $\bar{\alpha} / \alpha_f > 0.5$ is not satisfied. Note that this expansion is equivalent to neglecting the term proportional to $(h_w / h_f)^2$ in Eq. (31). Physically, the approximation is valid when a foam drains much less than 50% of its liquid content as it fills. We substitute Eq. (30) into Eq. (32) to obtain

$$\bar{\alpha}^2 \approx 2\alpha_f \left[\frac{\alpha_f h_f - h_w}{h_f - h_w} \right] - \alpha_f^2 \tag{33}$$

and substitute Eq. (33) into Eq. (27) to obtain

$$\frac{dh_w}{dt} = A\left[2\alpha_f \left[\frac{\alpha_f h_f - h_w}{h_f - h_w} \right] - \alpha_f^2 \right] - B\left[\frac{\alpha_f h_f - h_w}{\left[h_f - h_w \right]^2} \right] \left[\sqrt{\alpha_w} - \sqrt{\alpha_f} \right]. \tag{34}$$

To obtain a linear equation, we make the approximation $h_f >> h_w$. The maximum value of h_w is $\alpha_f h_f$, so the approximation is equivalent to α_f <<1. This approximation is valid for high-expansion foams, where α_f is typically 0.01 or less. Using this approximation, Eq. (34) can be expressed as

$$\frac{dh_w}{dt} = A\left[\alpha_f^2 - \frac{2\alpha_f h_w}{h_f} \right] - B\left[\frac{\alpha_f}{h_f} - \frac{h_w}{h_f^{\,2}} \right] \left[\sqrt{\alpha_w} - \sqrt{\alpha_f} \right]. \tag{35}$$

Putting Eq. (35) in standard form yields

$$\frac{dh_w}{dt} + \left[\frac{2A\alpha_f}{h_f} - \frac{B}{h_f^2} \left[\sqrt{\alpha_w} - \sqrt{\alpha_f} \right] \right] h_w = A\alpha_f^2 - \frac{B\alpha_f}{h_f} \left[\sqrt{\alpha_w} - \sqrt{\alpha_f} \right], \tag{36}$$

a linear ODE which can be solved analytically. For mathematical simplicity, we make one more approximation in the linear coefficient; we neglect the term $(B\left[\sqrt{\alpha_w} - \sqrt{\alpha_f} \right] / h_f^2)$. Since $h_f = h_{f0} + v_{inj} t$ is linear with respect to time, the term $2A\alpha_f h_f^{-1}$ is inversely proportional to t, whereas $B\left[\sqrt{\alpha_w} - \sqrt{\alpha_f} \right] h_f^{-2}$ is inversely proportional to t^2. Hence, the term

$B\left[\sqrt{\alpha_w}-\sqrt{\alpha_f}\right]h_f^{-2}$ quickly becomes much smaller than $2A\alpha_f h_f^{-1}$. The ordinary differential equation from which we obtain an analytical solution is therefore

$$\frac{dh_w}{dt}+\left[\frac{2A\alpha_f}{h_f}\right]h_w = A\alpha_f^2-\frac{B\alpha_f}{h_f}\left[\sqrt{\alpha_w}-\sqrt{\alpha_f}\right]. \tag{37}$$

Eq. (37) can be re-written as

$$\frac{dh_w}{dt} = A\alpha_f^2\left(1-2\frac{h_w}{\alpha_f h_f}\right)-\frac{B\alpha_f}{h_f}\left[\sqrt{\alpha_w}-\sqrt{\alpha_f}\right] \tag{38}$$

Eq. (38) indicates that the drainage rate will be equal to the difference between the drainage rate of a foam that has $\bar{\alpha}=\alpha_f$ (see Eqs. (26) and (24)) and a correction factor that depends on the "volume per cross section" ratio of the liquid lost to the liquid layer h_w to the total liquid added to the foam $\alpha_f h_f$. The correction factor accounts for the fact that $\bar{\alpha}$ decreases from α_f as liquid is lost from the foam to the liquid layer beneath. Intuitively, the ratio of the volume of liquid in the liquid layer to the volume of liquid in the foam layer will depend on how the rate of drainage compares with the rate by which the column is filling with foam. As shown below, the competition between these rates is captured in the analytical solution.

Equation (37) is in the form $dh_w/dt+\Phi(t)h_w=\Omega(t)$. Using the integration factor $\psi=\exp\left(\int\Phi(t)dt\right)$, the solution is given up to a constant by $h_w=\psi^{-1}\int\Omega(t)\psi\ dt$. The integration factor, using $dh_f=v_{inj}\,dt$, is

$$\psi=\exp\left(\int\frac{2A\alpha_f}{h_f}\,dt\right)=\exp\left(\frac{1}{v_{inj}}\int\frac{2A\alpha_f}{h_f}\,dh_f\right)=\exp\left(\frac{2A\alpha_f}{v_{inj}}\ln\left|h_f\right|\right)=h_f^{\frac{2A\alpha_f}{v_{inj}}}. \tag{39}$$

The solution is given by

$$
\begin{aligned}
h_w &= h_f^{\frac{-2A\alpha_f}{v_{inj}}}\left[\int\left[A\alpha_f^2-\frac{B\alpha_f}{h_f}\left[\sqrt{\alpha_w}-\sqrt{\alpha_f}\right]\right]h_f^{\frac{2A\alpha_f}{v_{inj}}}\,dt+C_2\right] \\
&= h_f^{\frac{-2A\alpha_f}{v_{inj}}}\left[\frac{A\alpha_f^2}{v_{inj}}\int h_f^{\frac{2A\alpha_f}{v_{inj}}}\,dh_f-\frac{B\alpha_f\left[\sqrt{\alpha_w}-\sqrt{\alpha_f}\right]}{v_{inj}}\int h_f^{\frac{2A\alpha_f}{v_{inj}}-1}\,dh_f\right]+C_2h_f^{\frac{-2A\alpha_f}{v_{inj}}} \\
&= h_f^{\frac{-2A\alpha_f}{v_{inj}}}\left[\frac{A\alpha_f^2}{v_{inj}}\left[\frac{v_{inj}h_f^{\frac{2A\alpha_f}{v_{inj}}+1}}{2A\alpha_f+v_{inj}}\right]\right]-h_f^{\frac{-2A\alpha_f}{v_{inj}}}\left[\frac{B\alpha_f\left[\sqrt{\alpha_w}-\sqrt{\alpha_f}\right]}{v_{inj}}\left[\frac{v_{inj}h_f^{\frac{2A\alpha_f}{v_{inj}}}}{2A\alpha_f}\right]\right]+C_2h_f^{\frac{-2A\alpha_f}{v_{inj}}} \\
&= \frac{A\alpha_f^2h_f}{2A\alpha_f+v_{inj}}-\frac{B\left[\sqrt{\alpha_w}-\sqrt{\alpha_f}\right]}{2A}+C_2h_f^{\frac{-2A\alpha_f}{v_{inj}}} \\
&= \left[\frac{1}{2+\frac{v_{inj}}{A\alpha_f}}\right]\alpha_fh_f-\frac{B\left[\sqrt{\alpha_w}-\sqrt{\alpha_f}\right]}{2A}+C_2h_f^{\frac{-2A\alpha_f}{v_{inj}}}.
\end{aligned}
\tag{40}
$$

We use the initial condition $h_w(0)=h_{w0}=0$ and $h_f(0)=h_{f0}$ at time $t=0$, which yields

$$
0=\left[\frac{1}{2+\frac{v_{inj}}{A\alpha_f}}\right]\alpha_fh_{f0}-\frac{B\left[\sqrt{\alpha_w}-\sqrt{\alpha_f}\right]}{2A}+C_2h_{f0}^{\frac{-2A\alpha_f}{v_{inj}}} \tag{41}
$$

which can be used to solve for the integration constant

$$
C_2=\left[\frac{B\left[\sqrt{\alpha_w}-\sqrt{\alpha_f}\right]}{2A}-\left[\frac{1}{2+\frac{v_{inj}}{A\alpha_f}}\right]\alpha_fh_{f0}\right]h_{f0}^{\frac{2A\alpha_f}{v_{inj}}}. \tag{42}
$$

Substitution of (42) into the final expression in (40) yields the analytical solution

$$h_w = \left[\frac{1}{2+\frac{v_{inj}}{A\alpha_f}}\right]\alpha_f h_f - \frac{B\left[\sqrt{\alpha_w}-\sqrt{\alpha_f}\right]}{2A} + \left[\left[\frac{B\left[\sqrt{\alpha_w}-\sqrt{\alpha_f}\right]}{2A} - \left[\frac{1}{2+\frac{v_{inj}}{A\alpha_f}}\right]\alpha_f h_{f0}\right] h_{f0}^{\frac{2A\alpha_f}{v_{inj}}}\right] h_f^{\frac{-2A\alpha_f}{v_{inj}}}$$

$$= \left[\frac{1}{2+\frac{v_{inj}}{A\alpha_f}}\right]\alpha_f v_{inj} t + \left[\left[\frac{1}{2+\frac{v_{inj}}{A\alpha_f}}\right]\alpha_f h_{f0} - \frac{B\left[\sqrt{\alpha_w}-\sqrt{\alpha_f}\right]}{2A}\right]\left[1-\left[\frac{h_{f0}}{h_{f0}+v_{inj}t}\right]^{\frac{2A\alpha_f}{v_{inj}}}\right]. \quad (43)$$

The value of $\bar{\alpha}$ during filling is found by substitution of Eq. (43) into Eq. (30).

Equation (43) can be simplified by neglecting h_{f0}. The abbreviated analytical solution for filling is given by

$$h_w \approx \left[\frac{1}{2+\frac{v_{inj}}{A\alpha_f}}\right]\alpha_f v_{inj} t - \frac{B\left[\sqrt{\alpha_w}-\sqrt{\alpha_f}\right]}{2A}. \quad (44)$$

For cases where the analytical solution is valid, the abbreviated solution given in Eq. (44) shows very little difference with the solution of (43) after roughly 10 seconds. The first term in the previous expression quickly becomes dominant during the filling process. This indicates that h_w has a predominantly linear time dependence, and therefore the drainage rate from the foam is approximately constant during filling. The first term in Eq. (44) contains $v_{inj}t$, which is the height of foam added from the start of filling to the time t. The liquid portion of the added foam is $\alpha_f v_{inj} t$. The coefficient

$$\left[\frac{1}{2+\frac{v_{inj}}{A\alpha_f}}\right] \quad (45)$$

is therefore a percentage of the added liquid that is drained (and added to h_w) at time t. For a given input liquid fraction α_f, the key parameters that determine this percentage are v_{inj} and A, which represent the time scales for filling and drainage, respectively. A key point of this study is that an appreciable amount of the added liquid can drain when the filling and drainage time scales are comparable. However, as one might expect, very little of the added liquid is drained during filling if one fills very fast such that $v_{inj} >> A\alpha_f$. The analytical solution is not valid for very slow foam injection such that $A\alpha_f >> v_{inj}$ because the condition for the validity of

the Taylor expansion of $\bar{\alpha}^2$ is not satisfied, i.e. $\bar{\alpha}$ will not be much less than 50% of α_f. However, the case can still be described by numerical solution of Eq. (31).

FREE DRAINAGE

For free drainage, we set $dh_f / dt = 0$ in Eq. (21) and integrate with respect to time to obtain

$$\bar{\alpha}\left(H - h_w\right) = -h_w + C_1, \tag{46}$$

where we solve for the integration constant

$$C_1 = \bar{\alpha}(t_0)\left(H - h_{w0}\right) + h_{w0}. \tag{47}$$

Note that free drainage occurs from a column of fixed height, H. Eqns. (46) and (47) simply state that the liquid content in the foam is equal to the difference between the initial liquid content and the amount of liquid that has drained out, causing the liquid layer to rise by the height $h_w - h_{w0}$.

We consider the general case for initial conditions on free drainage. Solving for $\bar{\alpha}$ in Eq. (46) yields

$$\bar{\alpha} = \frac{h_{w0} - h_w + \bar{\alpha}(t_0)\left[H - h_{w0}\right]}{H - h_w}. \tag{48}$$

Substituting the previous expression into Eq. (27) yields the free-drainage equation

$$\begin{aligned} \frac{dh_w}{dt} = A&\left[\frac{h_{w0} - h_w + \bar{\alpha}(t_0)\left[H - h_{w0}\right]}{H - h_w}\right]^2 \\ &- B\left[\frac{h_{w0} - h_w + \bar{\alpha}(t_0)\left[H - h_{w0}\right]}{\left[H - h_w\right]^2}\right]\left[\sqrt{\alpha_w} - \sqrt{\alpha_f}\right]. \end{aligned} \tag{49}$$

Eq. (49) can be solved numerically. However, we calculate an analytical solution that is nearly identical to the numerical solution for all cases examined in this study.

For free drainage, we change the dependent variable of the ordinary differential equation to $\bar{\alpha}$. Making this change allows the calculation of an analytical solution that is both simple to obtain and valid for a greater range of parameters than the solution obtained using h_w as the dependent variable. Differentiating Eq. (46) with respect to time yields

$$-\left[H - h_w\right]\frac{d\bar{\alpha}}{dt} = \frac{dh_w}{dt}. \tag{50}$$

We substitute the previous expression in Eq. (27) to obtain

$$\frac{d\bar{\alpha}}{dt} = -\frac{A\bar{\alpha}^2}{H - h_w} + \frac{B\bar{\alpha}}{\left[H - h_w\right]^2}\left[\sqrt{\alpha_w} - \sqrt{\alpha_f}\right]. \tag{51}$$

As in the filling case, we make the approximation that the height of the water layer is much less than the height of the foam column, $h_w << H$, and divide by $\bar{\alpha}^2$ in Eq. (51) to yield

$$\frac{1}{\bar{\alpha}^2}\frac{d\bar{\alpha}}{dt} = -\frac{A}{H} + \left[\frac{B\left[\sqrt{\alpha_w} - \sqrt{\alpha_f}\right]}{H^2}\right]\left[\frac{1}{\bar{\alpha}}\right]. \tag{52}$$

Using the relation

$$\frac{d}{dt}\left[\frac{1}{\bar{\alpha}}\right] = -\frac{1}{\bar{\alpha}^2}\frac{d\bar{\alpha}}{dt} \tag{53}$$

and defining $\eta \equiv 1/\bar{\alpha}$, we can express Eq. (52) as

$$\frac{d\eta}{dt} + \left[\frac{B\left[\sqrt{\alpha_w} - \sqrt{\alpha_f}\right]}{H^2}\right]\eta = \frac{A}{H}. \tag{54}$$

Eq. (54) is in the form $d\eta/dt + \Phi(t)\eta = \Omega(t)$. Using the integration factor $\psi = \exp\left(\int \Phi(t)dt\right)$, the solution is given up to a constant by $\eta = \psi^{-1}\int \Omega(t)\psi\ dt$. The integration factor is

$$\psi = \exp\left(\int \frac{B\left[\sqrt{\alpha_w} - \sqrt{\alpha_f}\right]}{H^2}dt\right) = \exp\left(\frac{B\left[\sqrt{\alpha_w} - \sqrt{\alpha_f}\right]t}{H^2}\right) \tag{55}$$

and the solution is given by

$$\begin{aligned}\eta &= \exp\left(\frac{-B\left[\sqrt{\alpha_w} - \sqrt{\alpha_f}\right]t}{H^2}\right)\left[\int \frac{A}{H}\exp\left(\frac{B\left[\sqrt{\alpha_w} - \sqrt{\alpha_f}\right]t}{H^2}\right)dt + C_2\right] \\ &= \frac{AH}{B\left[\sqrt{\alpha_w} - \sqrt{\alpha_f}\right]} + C_2\exp\left(\frac{-B\left[\sqrt{\alpha_w} - \sqrt{\alpha_f}\right]t}{H^2}\right).\end{aligned} \tag{56}$$

Using the initial condition $\eta\left(t_0\right) = 1/\bar{\alpha}\left(t_0\right)$ at time t_0,

$$\eta(t_0) = \frac{1}{\bar{\alpha}(t_0)} = \frac{AH}{B\left[\sqrt{\alpha_w} - \sqrt{\alpha_f}\right]} + C_2 \exp\left(\frac{-B\left[\sqrt{\alpha_w} - \sqrt{\alpha_f}\right]t_0}{H^2}\right) \tag{57}$$

yields the integration constant

$$C_2 = \left[\frac{1}{\bar{\alpha}(t_0)} - \frac{AH}{B\left[\sqrt{\alpha_w} - \sqrt{\alpha_f}\right]}\right] \exp\left(\frac{B\left[\sqrt{\alpha_w} - \sqrt{\alpha_f}\right]t_0}{H^2}\right). \tag{58}$$

The analytical solution for free drainage is therefore

$$\eta = \frac{1}{\bar{\alpha}} = \frac{AH}{B\left[\sqrt{\alpha_w} - \sqrt{\alpha_f}\right]} + \left[\frac{1}{\bar{\alpha}(t_0)} - \frac{AH}{B\left[\sqrt{\alpha_w} - \sqrt{\alpha_f}\right]}\right] \exp\left(\frac{-B\left[\sqrt{\alpha_w} - \sqrt{\alpha_f}\right]\left[t - t_0\right]}{H^2}\right) \tag{59}$$

and the corresponding value of h_w can be found by solving for $\bar{\alpha}$ in Eq. (59) and substituting in Eq. (48).

Let us examine a limiting case of Eq. (59). As t approaches infinity, we have

$$\frac{1}{\eta(\infty)} = \bar{\alpha}(\infty) = \frac{B\left[\sqrt{\alpha_w} - \sqrt{\alpha_f}\right]}{AH}. \tag{60}$$

The value of $\bar{\alpha}(\infty)$ is the equilibrium liquid fraction of the foam as predicted by the model. This expression for $\bar{\alpha}(\infty)$ could also be arrived at from Eq. (27) by using the condition $dh_w / dt = 0$ at equilibrium and the approximation $h_f = H >> h_w$.

We note that the average expansion ratio of the foam is given by $\overline{Ex} = 1/\bar{\alpha}$. We can express Eq. (59) as

$$\overline{Ex}(t) - \overline{Ex}(\infty) = \left(\overline{Ex}(t_0) - \overline{Ex}(\infty)\right) \exp\left(\frac{-B\left[\sqrt{\alpha_w} - \sqrt{\alpha_f}\right]\left[t - t_0\right]}{H^2}\right) \tag{61}$$

which shows that the foam progresses from its initial expansion ratio to that of equilibrium on an exponential time scale. Note that the exponent controlling the rate at which the initial expansion ratio progresses to equilibrium strongly depends on the height of the column; the process is slower for taller columns.

3.0 EXPERIMENTS

To generate foam, we created a liquid foam solution by mixing 2.2 parts concentrated liquid foam solution (Buckeye HXF 2.2% High-Expansion Foam Concentrate) with 97.8 parts distilled water. The surfactant solution is, by weight, 26% water, 29% hexylene glycol, 38% sodium laureth sulfate, and 8% proprietary mix of surfactants/stabilizers (refer to MSDS). We poured the solution into a liquid chamber and pressurized the chamber with nitrogen gas , N_2. The liquid solution was fed to the foam-generation device illustrated in Figure 6. The liquid solution entered the side of the foam generator and exited downward through a cone-patterned nozzle (Model 302-C, SureShotsSprayer.com) onto a copper screen with a diameter of 6.4 cm and 30x30 mesh cells per inch (40.8% open area) held in place by a rubber gasket. The N_2 pressure was increased in the liquid chamber such that the nozzle sprayed the liquid solution at a fixed volumetric rate of about 60 mL/minute, measured with a calibrated rotameter (Dwyer VFA-33 Visi-Float Flowmeter). An in-house source provided air flow into the top of the foam generator. A perforated plate and a bed of tightly packed, plastic straws, 6 cm long with an inner (outer) diameter of 0.25 cm (0.32 cm), conditioned the air flow for even distribution over the copper screen. Air flow rates of 8 L/min and 20 L/min, as determined by a mass-flow controller (Sierra Control Flo-Box Model # 905C-PS-BM-11), were used to generate foams with expansion ratios of 100 and 200, respectively.

A diagram of the drainage experiment is shown in Figure 6. Foam was generated beneath the foam-generation screen, moves through the foam generator, and exits into a 20-liter, transparent, plastic cylinder with a diameter of 0.213 m and a height of 0.561 m. The base of the cylindrical column was formed with a sheet of aluminum foil, sloped slightly downward toward the center, where a 1-cm diameter hole allowed the drained liquid to pass out of the cylinder. The liquid passing through the hole entered a funnel, collecting the drained liquid into a 500 mL graduated cylinder. A video camera recorded images of the liquid filling the graduated cylinder.

For each foam drainage experiment, the desired air flow was first set followed by the liquid. A stopwatch was used to record the times of key events. The liquid and air combined on the screen; the liquid foam solution was manually distributed on the screen to start foam generation. The excess liquid, mostly from the priming process before foam is formed, was collected in the passage beneath the screen. Foam exited the generator channel and traveled down the side of the cylinder. The beginning of the fill time was recorded when the foam moved past the specified height in the collection cylinder. Once the foam reached the bottom of the cylinder and touched the aluminum foil, a video camera began recording (Pinnacle Studio 12) the drained liquid collecting in a graduated cylinder. Once the foam filled the 20-liter cylinder, the fill time was recorded, the liquid and air flows were turned off, and the foam generator was set aside. A plastic lid was placed on top of the cylinder to minimize foam evaporation. The excess liquid in the channel below the foam-generation screen was collected and measured in a graduated cylinder.

The camera recorded video for about six minutes after the foam reached the base of the cylinder. The video recording was used to determine the amount of liquid drained versus time.

After six minutes, the drainage rate slowed significantly, allowing the accumulating liquid volume in the graduated cylinder to be measured by visual inspection. The volume of drained liquid was recorded at one-minute intervals until the change in volume was less than 2 mL/min. Subsequently, the drained liquid volume was measured in intervals of several minutes until the total drainage time reached about an hour. The foam was left in the cylinder overnight to completely drain, and this liquid volume was used to calculate the expansion ratio of the foam. Additionally, a value of the expansion ratio was also derived from the net amount of liquid sprayed into the foam during the filling process.

$$\text{Volume of liquid in foam} = \text{Liquid flow rate} \times \text{Fill time} - \text{Excess liquid} \tag{62}$$

$$Ex = \frac{\text{Total foam volume}}{\text{Volume of liquid in foam}} \tag{63}$$

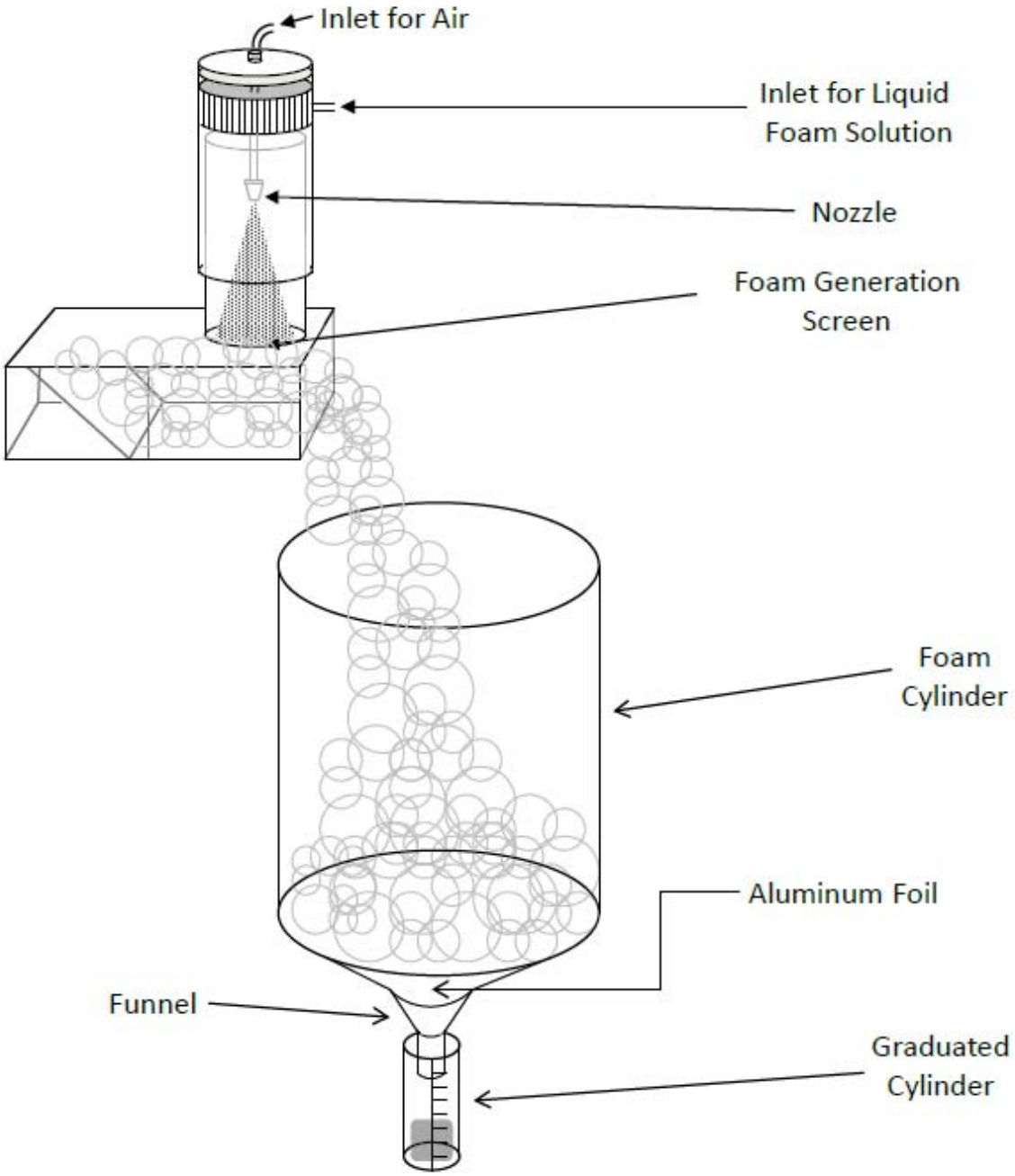

Figure 6: Experimental apparatus.

Foam bubble sizes were determined using photographs of the bubbles and a ruler taken at the top of the foam column immediately after filling. In Figure 7, an example photograph shows the centimeter-size bubbles characteristic of HiEx foams.

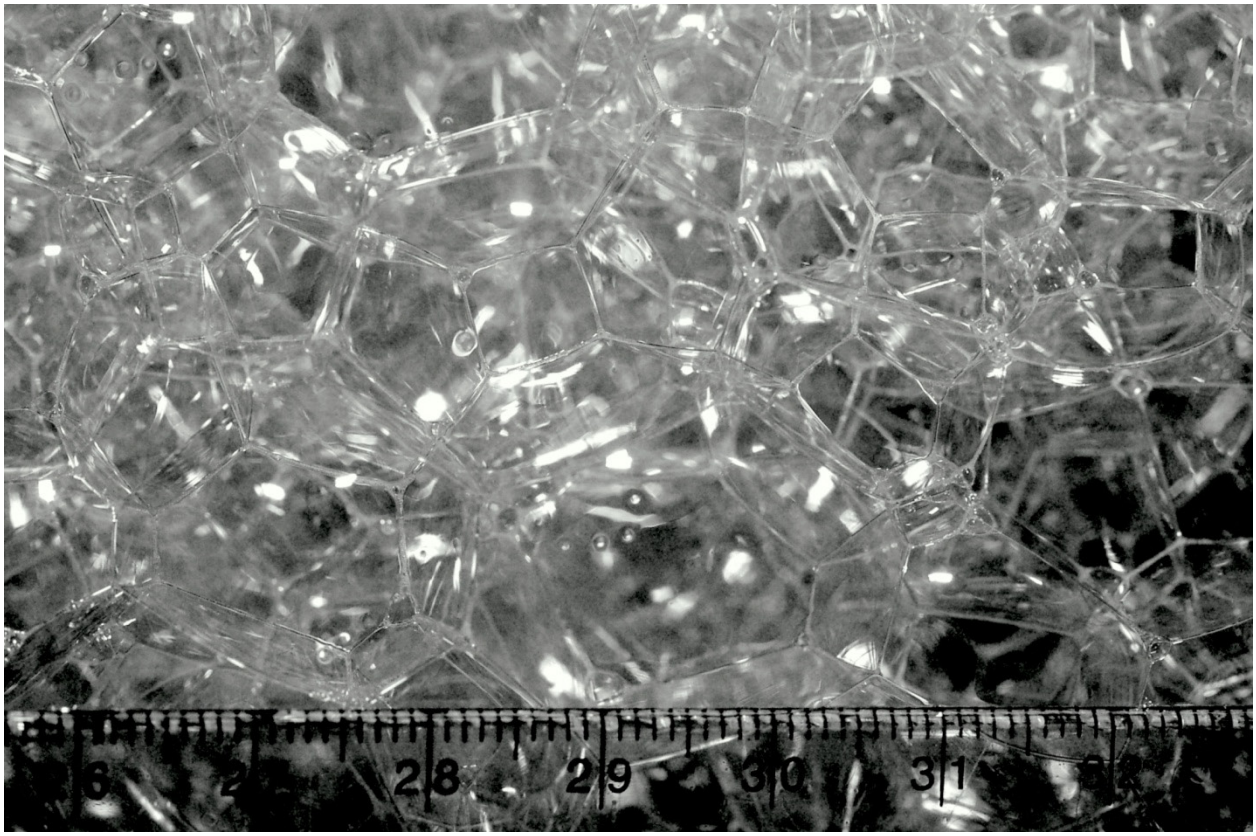

Figure 7: Photograph of foam bubbles for $Ex = 290$. The ruler markings are in centimeters.

The filling process in the experiment contrasts with the idealized filling process of the model, wherein the foam front has a uniform height as it travels upward. In the experiment, the foam flows into the cylinder and a portion of it slides along the cylinder wall as it travels downward. After it reaches the cylinder base, the foam takes a few seconds to reach the hole where liquid can drain into the graduated cylinder. The liquid draining from the foam must travel to the hole in the aluminum foil and accumulate to form a drop, and each drop must travel down the funnel and into the graduated cylinder.

The experiment and model also differ at the bottom boundary. In the model, liquid accumulates beneath the foam. In the experiment, liquid drained from the foam flows into a graduated cylinder beneath the foam column. The differences between the model and experiment are discussed below.

The liquid layer under the foam in the model allows liquid to be transported back into the foam from the water layer beneath. Capillary suction is a physical phenomenon that occurs when the pressure of the liquid in the foam is less than the pressure of the liquid with which it comes into contact. The suction of liquid can occur in the model at the beginning of the filling process to some extent, depending on the parameters of the foam. In the experiment, however, there is no liquid layer beneath the foam. Under the experimental conditions, the

model predicts that there only would be a small amount of liquid drawn into the foam over a short period of time were the foam sitting on liquid. However, for much smaller bubble sizes and/or much greater expansion ratios than were experimentally studied, the model predicts that capillary suction is no longer negligible. Boundary conditions have been included in other modeling works [8,9] to eliminate capillary suction and introduce an induction period during which liquid does not drain from the foam. Because the amount and duration of capillary suction predicted by the model for the experiments of this work are very small, we do not correct the boundary conditions to eliminate the suction.

The liquid drained during filling is enough to form a very small liquid layer beneath the foam as it drains; thus the experimental bottom boundary condition during filling should be similar to that of the model. However, the experimental foam may not have a thin layer of liquid present during the free drainage period. As a result, the model could slightly overpredict the effect of capillarity during the free drainage process. Additionally, the model considers the reduction of the length of the foam layer due to the increasing height of the water layer. The corresponding reduction in height is negligible for HiEx foams because the height of the water layer is very small compared to the height of the foam layer, i.e. $h_w << h_f$. This is an approximation made in the analytical solutions of the model.

Finally, the foams generated in experiments have a distribution of bubble radii, whereas the model assumes all bubbles are equal in size. A direct comparison between polydisperse and monodisperse foams is not possible, and it is not clear what averaging procedure will provide a mean bubble radius that will correlate with the experimental drainage data for the polydisperse foam. Magrabi et al. [8] propose that the appropriate average bubble size is calculated from the bubble-size dependence of the liquid flow rate through a channel. In their work, the average liquid flow rate through a channel in a polydisperse foam is calculated by the fourth moment of the bubble radius distribution because the flow rate is proportional to the fourth power of the bubble radius. In our experiments, we did not obtain a reliable bubble-size distribution function that would enable us to calculate an average bubble radius. Instead, we adjusted the bubble radius to fit the experimental data for each foam, and the bubble radius obtained from the fit was compared to the range of bubble radii obtained from photographs such as that shown in Figure 7. For all experiments, the bubble radius obtained from the fit was within the range of bubble radii observed in the photographs.

4.0 RESULTS AND DISCUSSION

An example case of foam drainage during filling is shown in Figure 8. At the start of filling, there is a relatively large pressure gradient caused by the small foam height and boundary conditions on α that competes with gravity. The drainage behavior during this initial period strongly depends on the choice of parameters. As the foam height increases, the force of gravity becomes dominant and drives liquid out of the foam. A constant drainage rate from the foam quickly develops, and the height of the water layer increases linearly with time. During this period, the average liquid fraction of the foam decreases to a steady-state value. For the

example case shown, the average liquid fraction decreases from an input value of 0.005 $(Ex = 200)$ to a steady-state value of about 0.00425 $(Ex = 235)$. The foam loses about 15% of its original liquid during the filling process.

Under other conditions, such as slower injection velocities, very high expansion ratios, and/or small bubble sizes, h_w decreases from zero at the beginning of the filling process. During this time, the pressure gradient dominates gravity and causes liquid suction into the foam from the water layer beneath. This behavior is also reflected in the behavior of $\bar{\alpha}$, which rises above its initial value at the start of filling.

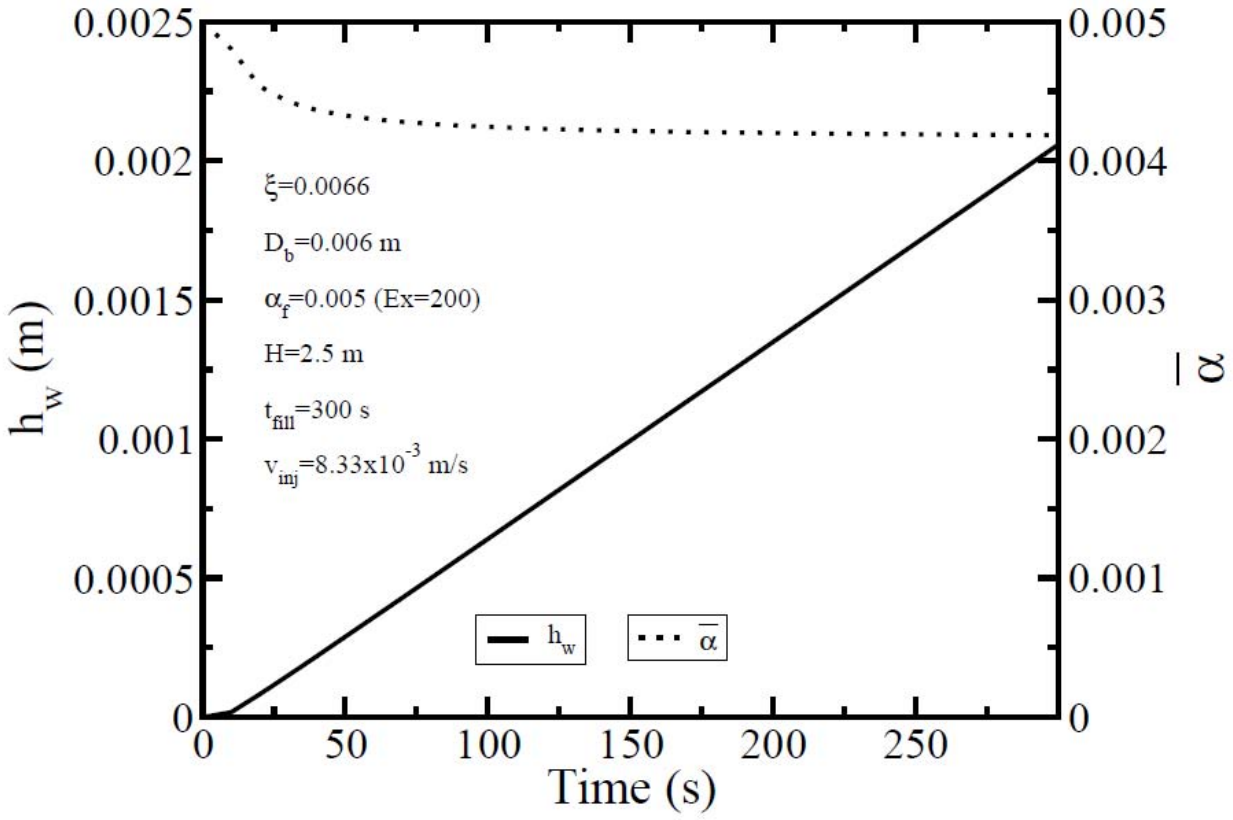

Figure 8: Model prediction of liquid drained during foam filling.

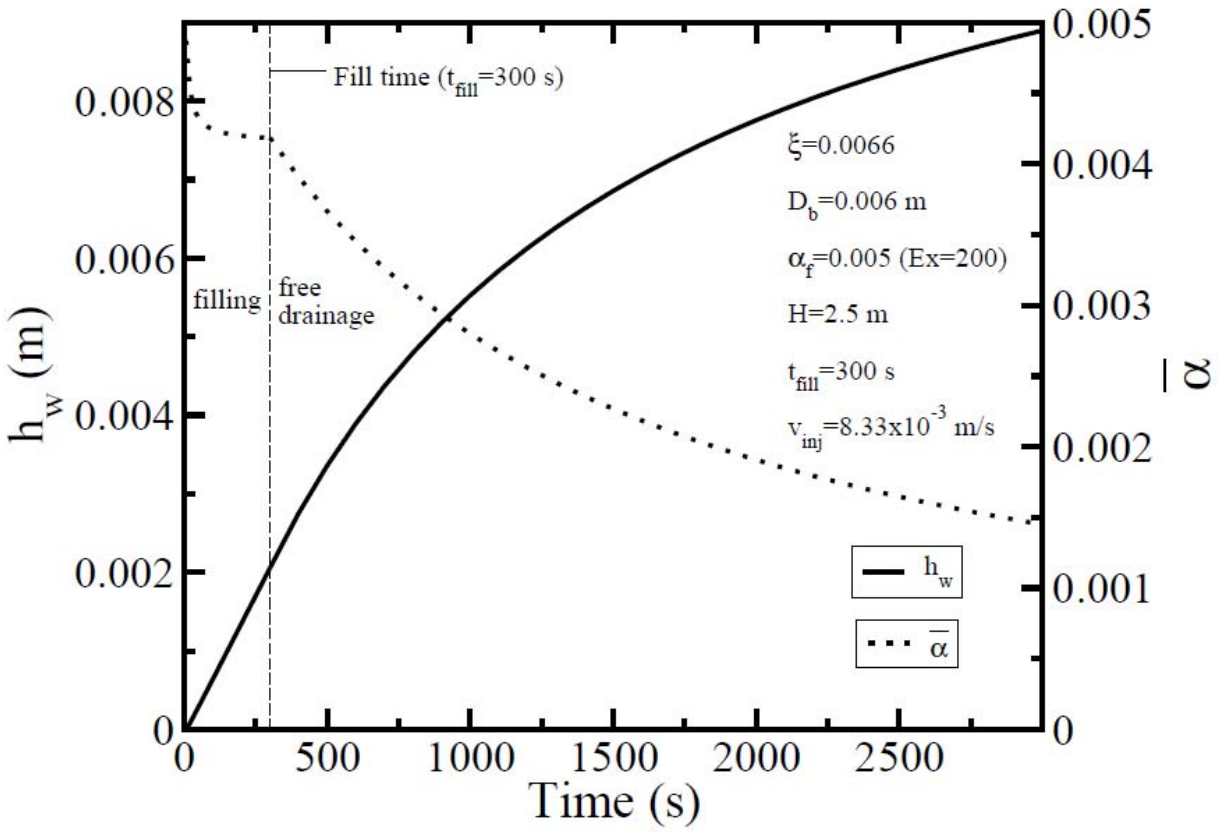

Figure 9: Model prediction of liquid drained during and after foam filling.

At the end of filling, the free drainage period begins. Figure 9 extends the computation in Figure 8 to include the free drainage behavior after filling. The foam continues to drain, but is no longer receiving liquid from input foam. When filling is ceased, the drainage rate begins to decrease slightly and the average liquid fraction decreases abruptly. In the foam, the channels contract in response to the reduced liquid content, and the drainage rate will approaches zero as the driving forces for liquid flow come into equilibrium. During this process, the height of the water layer approaches its equilibrium value at an exponential rate, and the average liquid fraction behaves in a similar fashion.

The analytical solutions of this work are valid only for a subset of the conditions for which their original differential equations can be solved by numerical methods. For the filling case, the approximations made in the analytical solution are valid when the average liquid fraction decreases from the input liquid fraction by much less than 50%. It is difficult to predict *a priori* when this condition will be satisfied. To show the important parameters to consider when deciding whether to use the analytical solution, we consider Eq. (30) when $h_w << h_f$ and the linear term in Eq. (43) to yield the approximation

$$\bar{\alpha} \approx \alpha_f - \frac{h_w}{h_f} \approx \alpha_f \left(1 - \frac{1}{2 + \frac{v_{inj}}{A\alpha_f}} \right) = \alpha_f \left(\frac{1 + \frac{v_{inj}}{A\alpha_f}}{2 + \frac{v_{inj}}{A\alpha_f}} \right). \quad (64)$$

From the previous expression, it can be seen that the quantity affecting the reduction in $\bar{\alpha}$ from the input liquid fraction is $v_{inj} / A\alpha_f$. By comparison of the drainage rate as predicted by the numerical and analytical solutions, we see that the difference for Ex up to 200 is around 2% when we use the condition $v_{inj} / A\alpha_f \approx 5$. Note that for Ex up to 600, a slightly greater value of 8 is needed to achieve the same accuracy. Substitution of this value in Eq. (64) indicates that the average liquid fraction should not decrease from the input value by much more than about 15% for the analytical solution to maintain this accuracy. For our experiments, the value of $v_{inj} / A\alpha_f$ ranges from about 0.5 to 2, and the analytical solution does not provide the drainage rate with sufficient accuracy.

It is important to note that the analytical expression is valid for field cases, where the fill rate is much faster. For a foam delivered to a room with a standard ceiling height of $H \approx 2.5\, m$ that must be filled within $120\, s$, one obtains $v_{inj} / A\alpha_f \approx 10$ when using conditions similar to our experimental values, $A \approx 0.45\, m/s$ and $\alpha_f = 1/200$. In Figure 10, we show how the analytical solution compares with the numerical solution for bench-scale and large-scale values of $v_{inj} / A\alpha_f$.

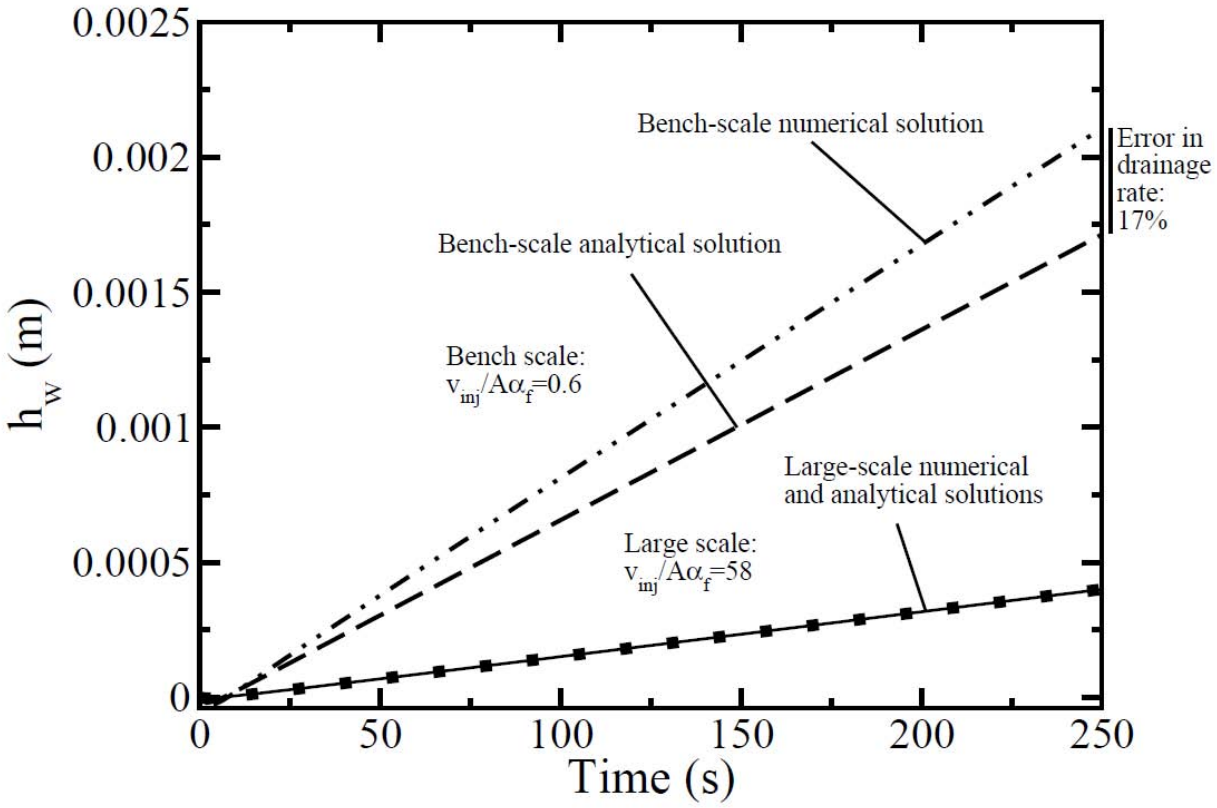

Figure 10: Comparison of numerical and analytical solutions for the height of the liquid layer as a function of time during filling for large-scale and bench-scale conditions. The parameters for the large scale are $v_{inj} = 0.05\ m/s$ and $\alpha_f = 0.002$. The large-scale injection velocity is calculated based on a 6 m column height and a 120 s fill time. The parameters for the bench scale are $v_{inj} = 0.0022\ m/s$ and $\alpha_f = 0.0083$. In both calculations, the parameters $\xi = 0.0066$ and $D_b = 0.006\ m$ are used.

The analytical solution for free drainage is in excellent agreement with the numerical solution to the original differential equation. In Figure 11, we show the drainage behavior for different bubble sizes in the case of initial $Ex = 200$; the solutions are nearly identical. Initial expansion ratio values were also varied independently of bubble size from $Ex = 20$ to 600 and the same excellent agreement was obtained.

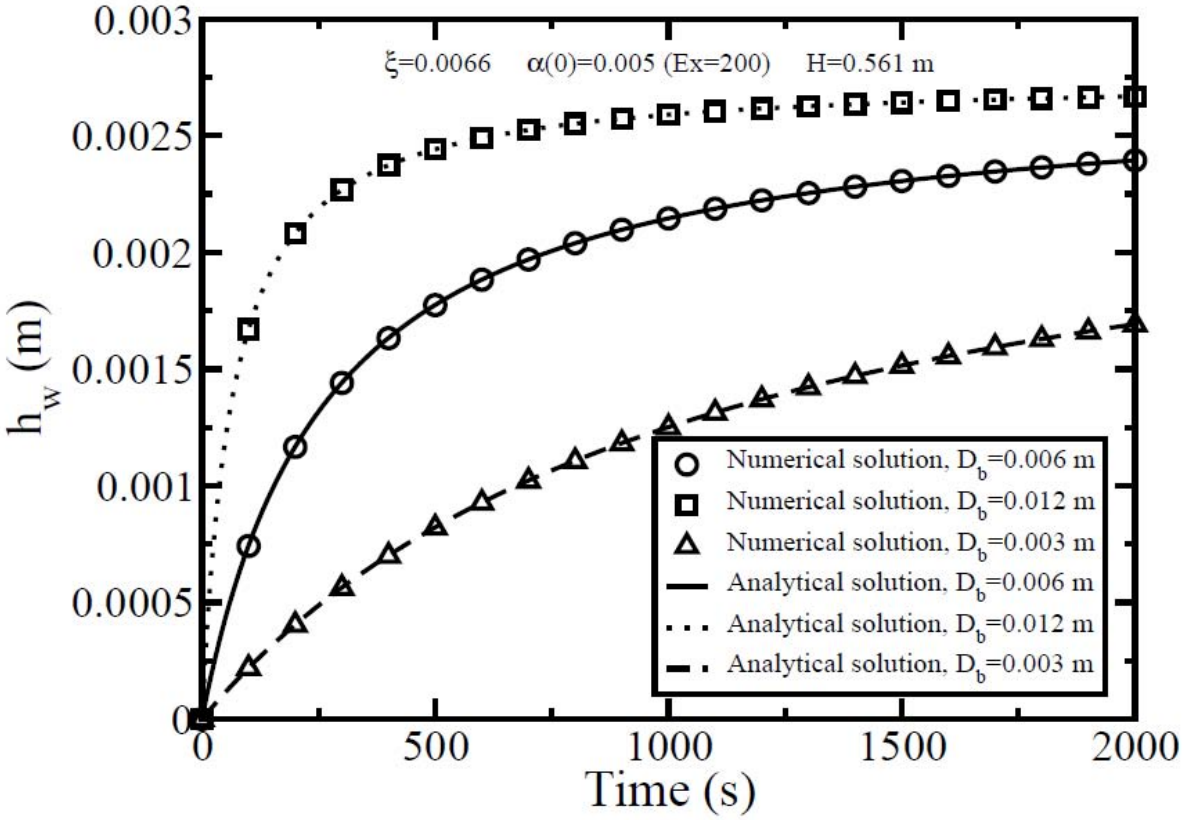

Figure 11: Comparison of numerical and analytical solutions for the height of the drained liquid for free drainage for different bubble sizes.

Shown in Figure 12 is a comparison of solutions for filling and free drainage combined. The analytical solutions using the large-scale parameters are identical to the numerical solutions. However, the analytical solutions calculated with the bench-scale parameters exhibit significant differences during both filling and free drainage periods. The overprediction for drainage during filling is responsible for the underprediction in the free drainage period compared to the numerical solution. The initial conditions for h_w and $\bar{\alpha}$ in the analytical free-drainage solution are equal to the corresponding values of the filling analytical solution at the end of the filling process. Hence, it is necessary to accurately calculate the filling solution to also accurately predict the magnitude of the liquid drained during the free-drainage period.

The model indicates that the drainage rate from the filling solution approaches the initial drainage rate of the free drainage solution at large values of $v_{inj} / A\alpha_f$. The difference between the initial drainage rates at $v_{inj} / A\alpha_f = 20$ is about 10%, and at $v_{inj} / A\alpha_f = 40$, the difference is about 5%. This suggests that filling can be ignored at very high injection velocities because the analytical free-drainage solution provides a reasonable approximation to the entire drainage process.

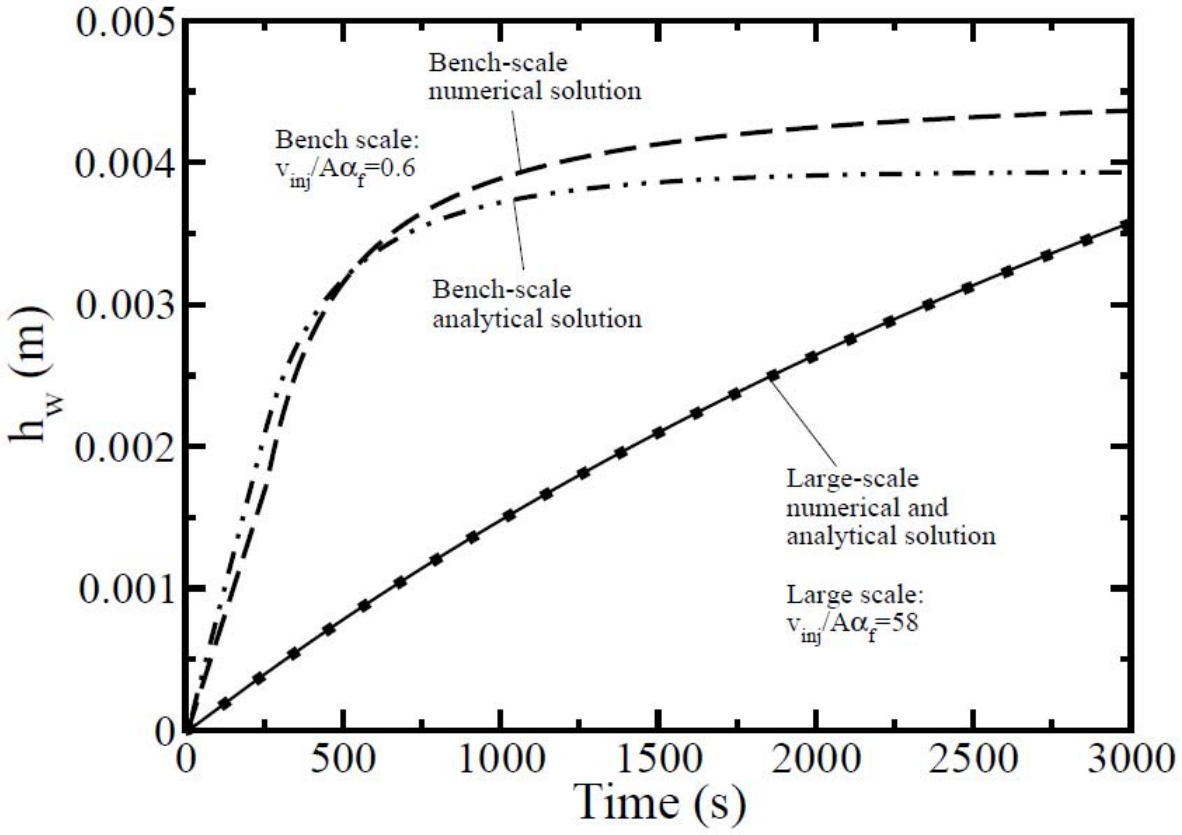

Figure 12: Comparison of numerical and analytical solution both during and after the filling process. The parameters for the large scale are $v_{inj} = 0.05\ m/s$, $t_{fill} = 120\ s$, $H = 6\ m$, and $\alpha_f = 0.002$. The parameters for the bench scale are $v_{inj} = 0.0022\ m/s$, $t_{fill} = 259\ s$, $H = 0.561m$, and $\alpha_f = 0.0083$. In both calculations, the parameters $\xi = 0.0066$ and $D_b = 0.006\ m$ are used.

The analytical solutions of this work, containing many approximations, can be used to calculate drainage behavior in good agreement with numerical solutions of the partial differential equations from which the model is derived. To show this, we compare our results with those of another model that has been used to describe free drainage, that of Magrabi et al. [8], which uses similar starting equations.

Magrabi et al. [8] studied free drainage from foam with an initial expansion ratio of 20 ($\alpha = 0.05$). In Figure 13, we compare their modeling results with modeling results using our simplified analytical solution for free drainage. The parameters are listed in Appendix B.

For comparison, we use the data from Ref. [8] for the mass of water drained as a function of time to calculate the corresponding value of h_w, the volume of liquid drained per

unit area of the foam column used in the experimental work. Using the liquid density and foam-column geometry reported in Ref. [8], we transform the drained-mass data to water height via

$$h_w(t) = \frac{V_d(t)}{S} = \frac{M_d(t)}{\rho \pi R^2} \tag{65}$$

where $V_d(t)$ is the volume of liquid drained from the foam, S is the cross-sectional area of the foam column, $M_d(t)$ is the mass of liquid drained, ρ is the intrinsic liquid density, and R is the radius of the cylindrical foam column.

We shifted by the respective induction times as reported in Ref. [8] of Magrabi et al. In the work, there was a no-flow boundary condition at the bottom of the foam column until that boundary reached a liquid fraction of 0.26. Our model, however, has a constant bottom boundary condition of $\alpha_w = 0.26$. The induction time predicted by our model is much smaller, in comparison.

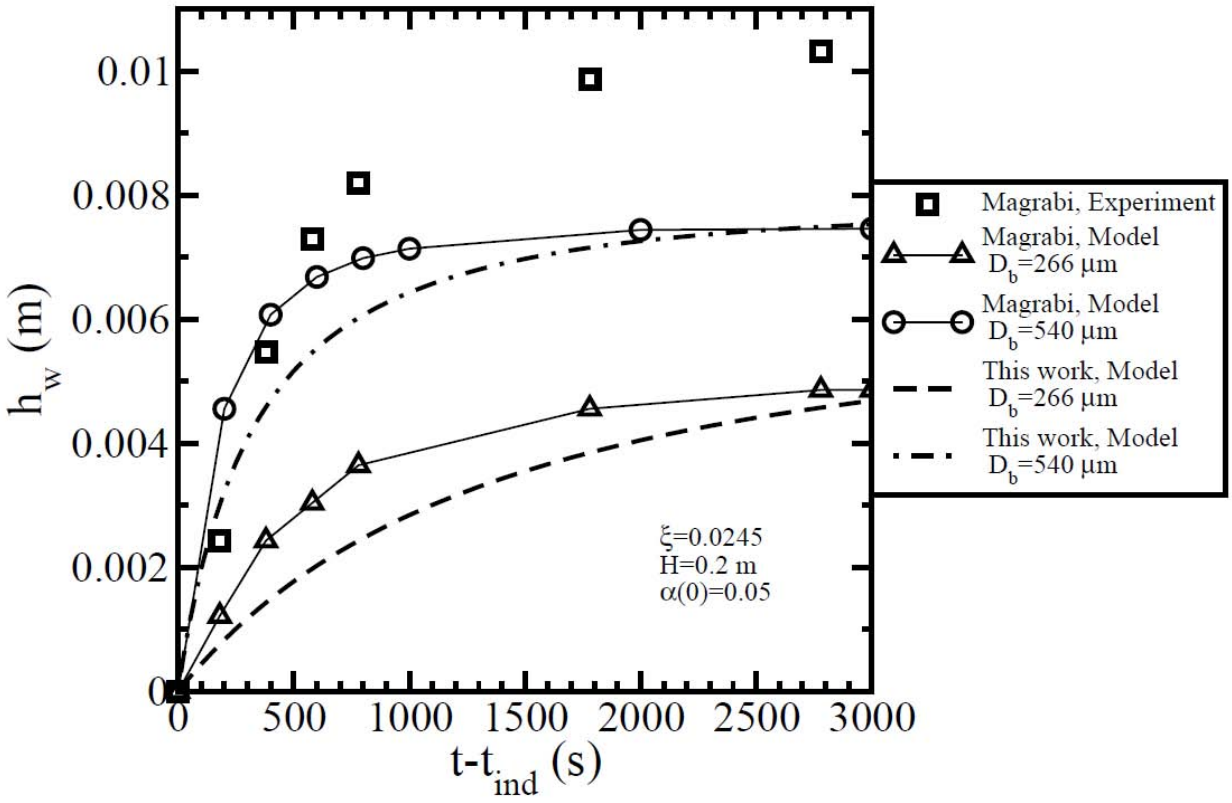

Figure 13: Height of drained liquid for free drainage (experimental and modeling results from Ref. [8] and modeling results of this work). The induction time of Ref. [8] is $t_{ind} = 240\ s$ .for $D_b = 266\ \mu m$ and $t_{ind} \approx 20\ s$ for $D_b = 540\ \mu m$. The induction time for our modeling results is $t_{ind} = 0\ s$.

As shown in Figure 13, the experimental data of Ref. [8] disagree with the predictions of their model. The authors argue that coarsening is the effect responsible for the disagreement, which is supported by measurements of average bubble radius that increase significantly during the first 960 s after foam formation. The effect of coarsening was not considered in their model, but it was shown that by increasing the bubble size from the initial value to the value measured after 960 s, the model predicts a greater drainage rate that increases the agreement with the experimental data. However, bubble sizes are difficult to measure during drainage because the distribution evolves over time. Further, the physics responsible for the evolution of bubble size in foam is not well understood.

Although our model calculations of their conditions show disagreement with their experimental data, our modeling calculations are in reasonable agreement. The experimental foam in Ref. [8] contained a low expansion ratio of 20 and a bubble diameter less than a millimeter; our model was designed specifically to treat high-expansion foams $(Ex > 100)$ with bubble diameters ranging from several millimeters to a few centimeters. Coarsening will have much less of an effect on the drainage behavior for our foams with bubble diameters an order of magnitude larger. Additionally, our model predicts a smaller drainage rate than their model. The largest contribution to the difference in the model predictions is that we consider the length-averaged behavior of the liquid volume fraction and liquid velocity by integrating the conservation equations. The resulting simplification of the model was expected to introduce some error. However, the clear advantage of considering the average behavior is that it allows the calculation of analytical solutions to describe the drainage behavior as a function of time.

The liquid fraction predictions of the two models are compared in Figure 14. The figure shows how the height-averaged liquid fraction predicted in this work compares to the predictions of a height-resolved model at various heights within a column. From visual inspection, our analytical solution appears to capture the length-averaged behavior reasonably well.

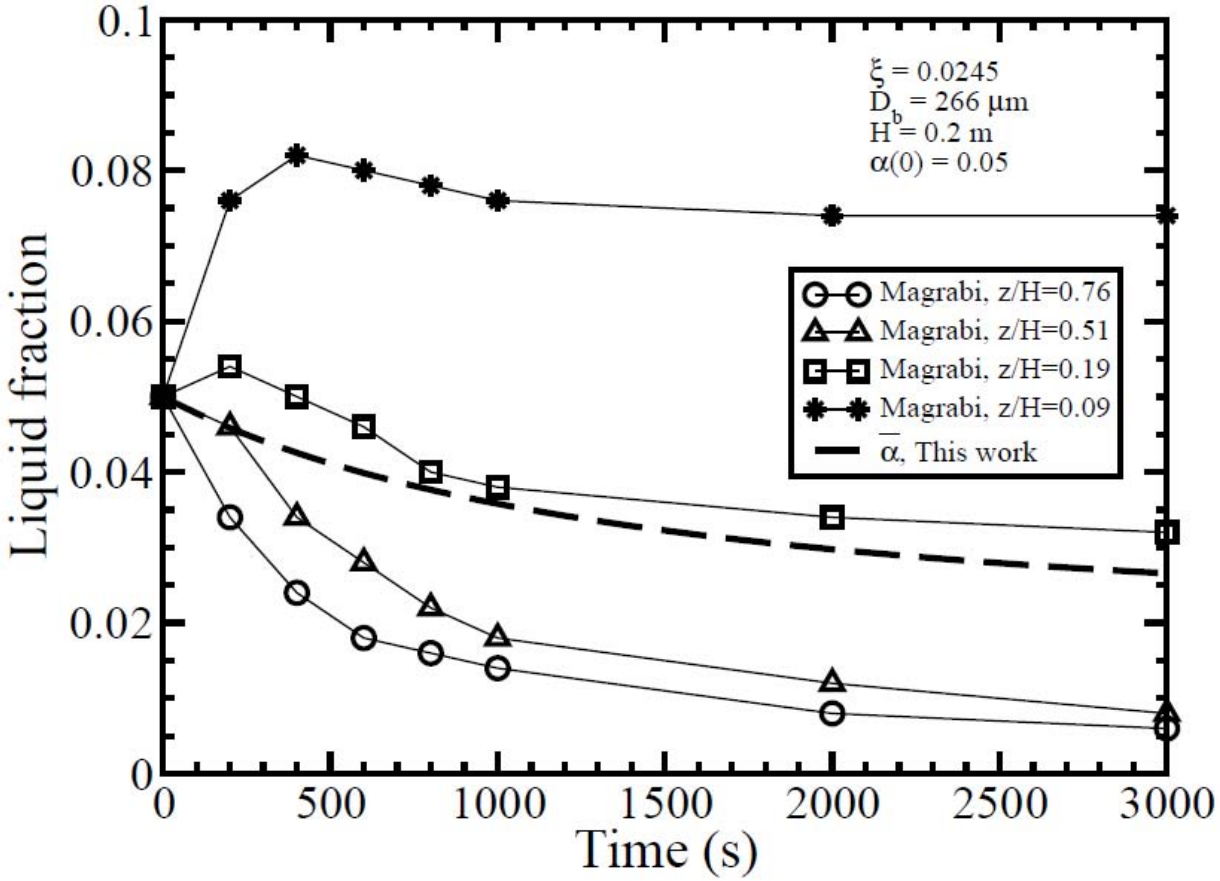

Figure 14: Comparison of length-averaged liquid fraction $\bar{\alpha}$ of this work with model predictions of liquid fractions at four positions along the height of the column from Ref. [8]. Note that z/H=0 is the bottom of the column and z/H=1 is at the top.

Next, we provide a comparison of our model with experimental drainage measurements during both filling and free drainage. We reiterate that the analytical solution for filling is not valid for the relatively slow injection velocities in the bench-scale experiments of this work, although it is valid for large-scale field conditions. Therefore, during the filling portion of the experiments, we numerically solve Eq. (31) to obtain h_w as a function of time from $t = 0$ until the fill time. On the other hand, the analytical solution for free drainage is valid for the bench-scale experiments, and we use the analytical solutions for t greater than the fill time.

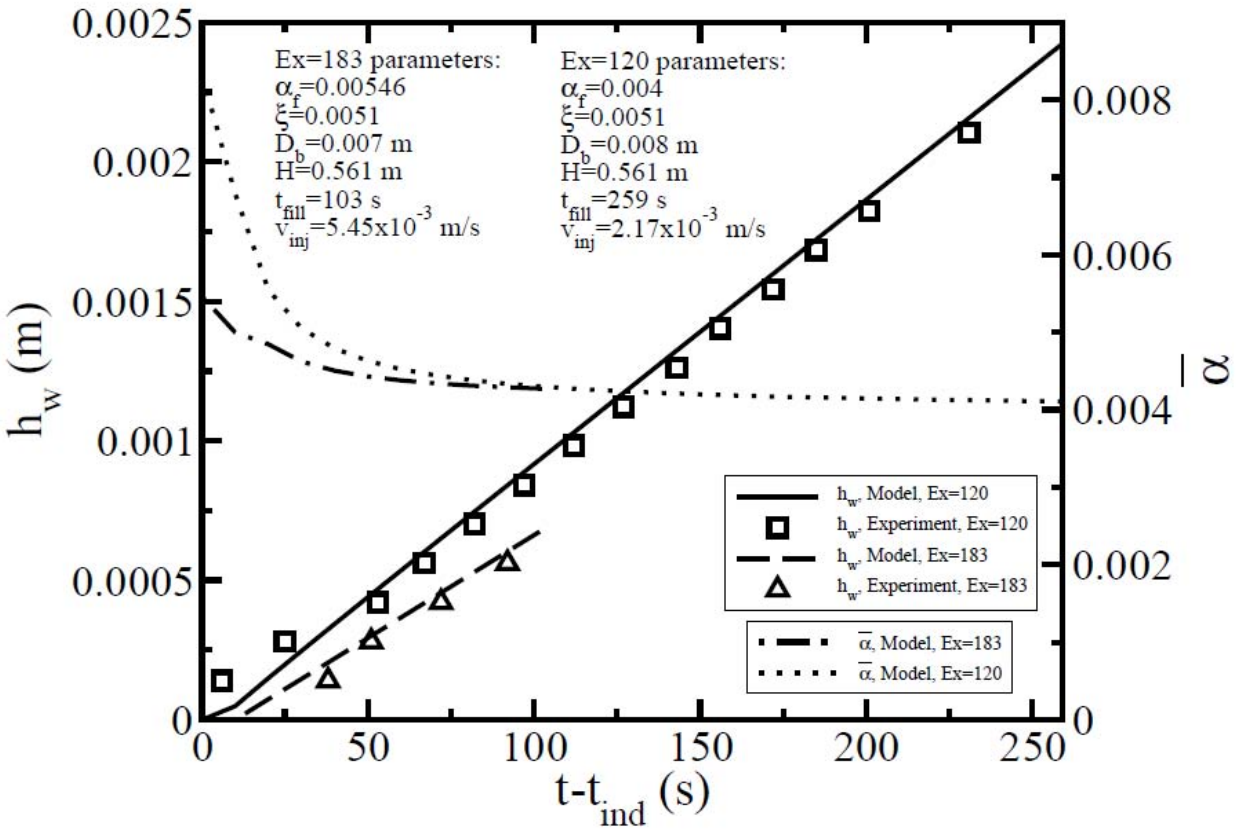

Figure 15: Comparison of model and experiment during the foam-filling period. The induction time is denoted t_{ind} .

The modeling and experimental data of this study for filling are shown in Figure 15. The experimental data suggest that the height of the water layer increases linearly with time, as predicted by the model. Note that there is an induction time of approximately 20 s in the experiments of this work, but the model underpredicts this value.

Note the appreciable drainage that occurs during filling in Figure 15. For the Ex=183 case, the length-averaged liquid fraction decreases from about 0.0055 $(Ex = 183)$ to approximately 0.00425 $(Ex = 235)$ during the filling period of 103 s. In the $Ex = 120$ case, the liquid fraction decreases from 0.0083 $(Ex = 120)$ to about 0.0046 $(Ex = 217)$ during the filling period of 259 s. The expansion ratio increases by about 28% and 81%, respectively, during the filling period. This shows that the drainage occurring during the filling process can significantly affect the expansion ratio of the foam.

The model contains the adjustable parameter ξ. We assume that the HiEx foams of this study have immobile channel walls and we use a permeability constant for these conditions that has been calculated in Ref. [7]. Also, the bubble diameter for the model calculations is fit to

the experimental data of liquid drained versus time. We fit the filling portion of the experimental drainage curve because we use a modified Hagen-Poiseuille equation, valid for fully developed, steady-state flow. There is a wide distribution in the experimental bubble size, ranging in diameter from about a millimeter to a couple of centimeters. The average bubble size from fitting the experimental data was shown to be within the bubble-size distribution from the photographs. The effect of bubble size on drainage behavior is examined below and the bubble-size range within the distribution observed in the experiments is investigated.

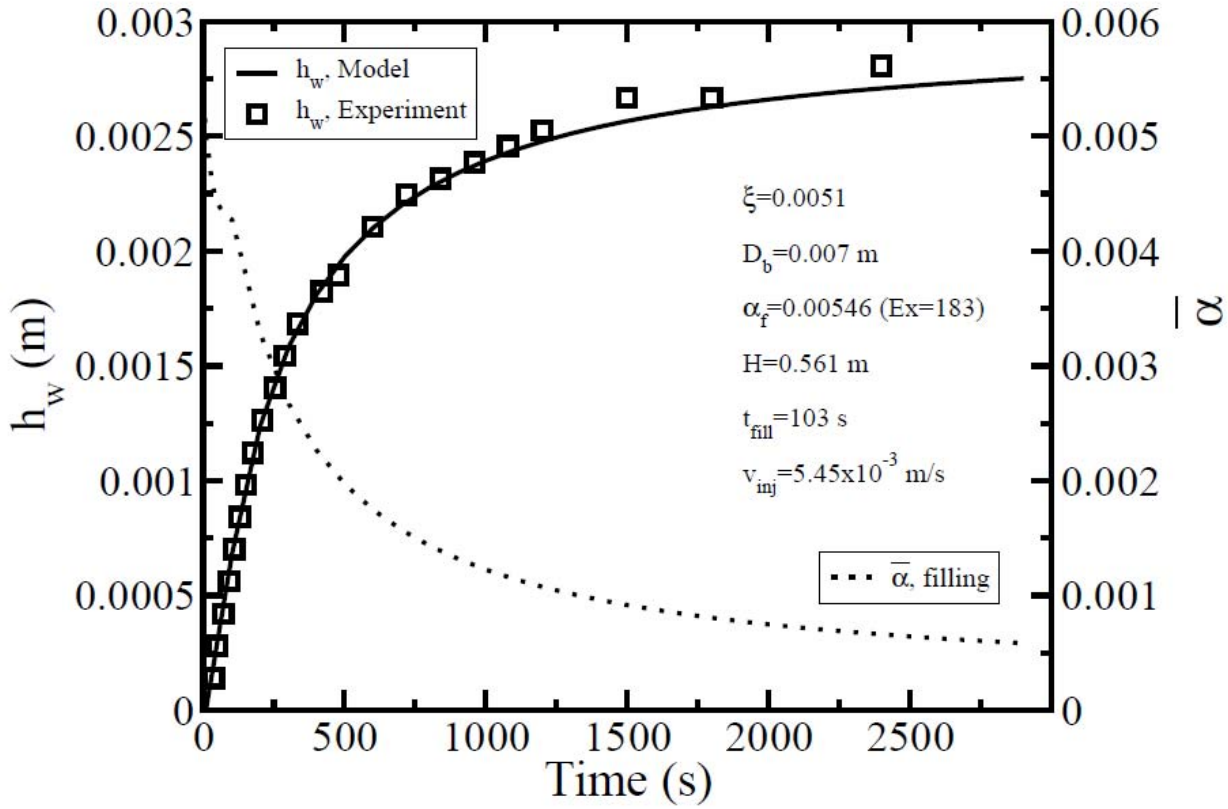

Figure 16: Comparison of model with experimental data for Ex= 183 for filling and free drainage periods.

The experimental data and model predictions for the entire drainage period including both filling and free drainage are shown in Figure 16 and Figure 17 for the cases of $Ex = 183$ and $Ex = 120$, respectively. After the filling period, the drainage rate in the experiment decreases. Good agreement is shown between the model and experiment during the free drainage period, which suggests that the data fits well to the exponential dependence of the model.

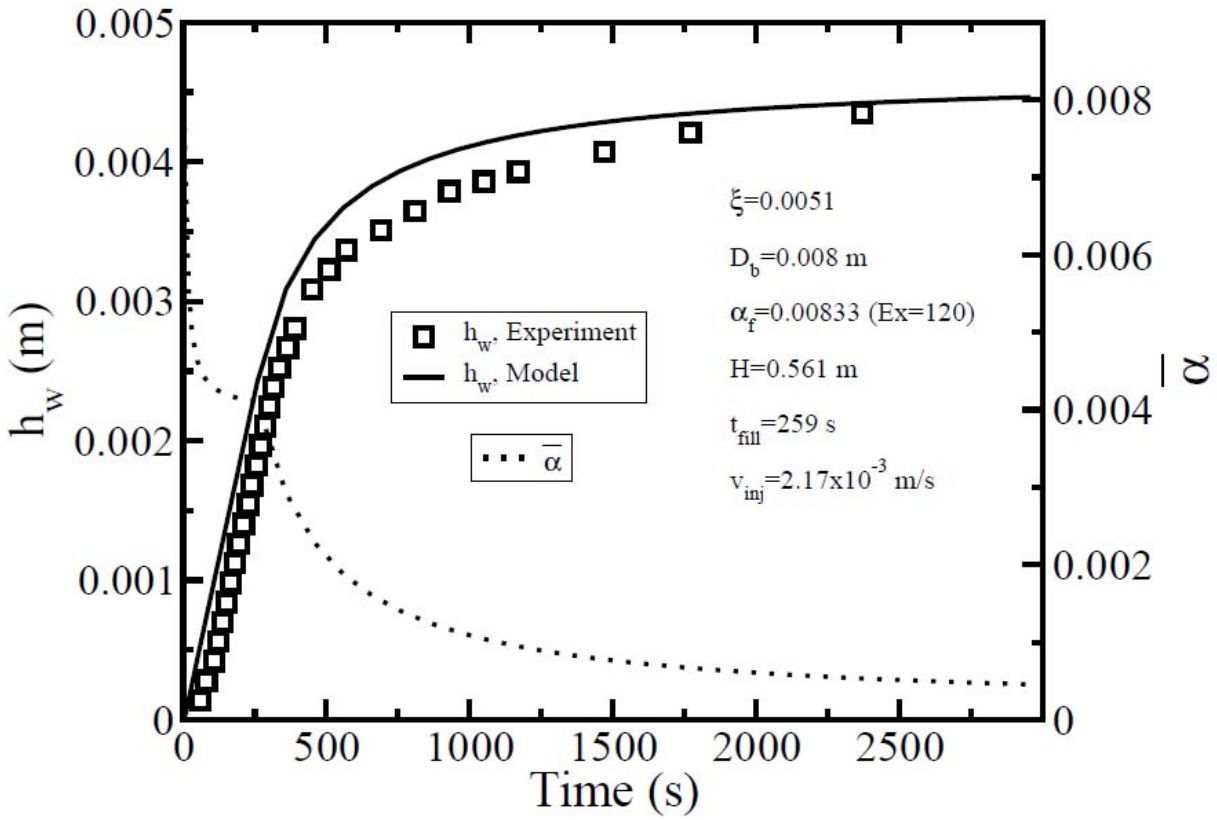

Figure 17: Comparison of model and experimental data for Ex=120 during filling and free drainage periods.

Comparison of model and experiment results of this work show better agreement than the model and experiment results comparison of Magrabi et al [8]. In the latter, the predicted value of h_w at equilibrium is 50% smaller than the experimental value. Our predicted value of h_w at equilibrium is very close to the experimental value. To understand the difference, we compare the ratio of the equilibrium average liquid fraction to the initial liquid fraction for the two experiments. We use Eq. (60) to calculate

$$\frac{\bar{\alpha}(\infty)}{\bar{\alpha}(0)} = \frac{B\left[\sqrt{\alpha_w} - \sqrt{\alpha_f}\right]}{AH\bar{\alpha}(0)} = \frac{\gamma\sqrt{\delta}\left[\sqrt{\alpha_w} - \sqrt{\alpha_f}\right]}{L\rho g H\bar{\alpha}(0)} \quad . \tag{66}$$

Note that this is also equal to the ratio of the liquid volume of the foam at equilibrium to the initial liquid volume in the foam. Using the parameters of Magrabi et al. [8] for a bubble radius of 133 μm and $\sqrt{\alpha_f} << \sqrt{\alpha_w}$, this ratio is approximately 0.5; only 50% of the water is drained from the foam. Note that the equilibrium experimental value in Ref. [8] is approximately equal to $\bar{\alpha}(0)H = 0.05 \times 0.2\, m = 0.01\, m$, the total liquid volume in the foam per unit area of the foam

column, and therefore the experiment indicates that nearly 100% of the liquid in the foam is drained at equilibrium. The prediction of the percent of liquid drained at equilibrium using Eq,. (66) is consistent with the model data shown in Figure 13; the value of h_w is about 50% of the experimental value. On the other hand, this ratio is approximately 0.02 for the parameters of this study; only 2% of the initial liquid remains in the foam. The main contribution to the difference in the $\bar{\alpha}$ values is the very large difference in bubble size between the two studies.

Table 2: Model parameters for comparison with experimental data.

γ	Surface tension	$2.25\times10^{-2}\ \frac{N}{m}$
μ	Liquid viscosity	$8.94\times10^{-4}\ \frac{kg}{m\ s}$
ξ	Permeability constant	0.0051
ρ	Liquid density	$997\ \frac{kg}{m^3}$
α_w	Liquid fraction at foam/liquid interface (mass balance)	1
α_w	Liquid fraction at foam/liquid interface (momentum balance)	0.26

Table 3: Initial conditions for filling solution

h_{w0}	Initial height of liquid layer	$0\ m$
h_{f0}	Initial height of foam layer	$0.01\ m$
t_0	Starting time	$0\ s$

An advantage of the analytical solutions of this work is that they can be used to easily fit the permeability coefficient to experimental data for a given foam. In this work, the permeability coefficient appears to be constant between two experiments where the expansion ratio is varied from 183 to 120 and the fill time is varied from 103 s to 259 s in a foam column of height 0.561 m. Further work is necessary to determine the range in foam parameters for which the permeability coefficient remains approximately constant. Note that previous models [6,7] which assume that the viscous force is predominantly located in channels with immobile walls also have an effective permeability coefficient that is constant, regardless of foam parameters.

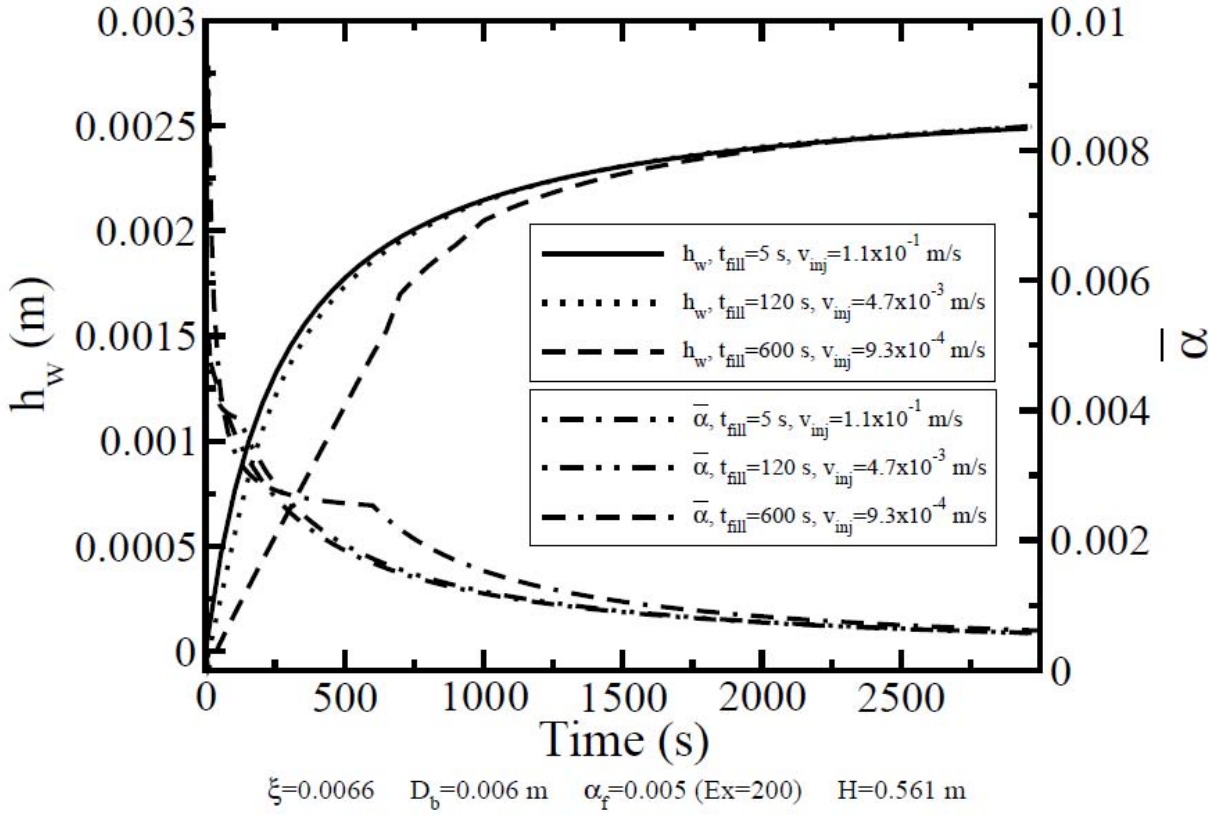

Figure 18: Effect of fill rate on drainage.

EFFECT OF MODEL PARAMETERS ON FOAM DRAINAGE BEHAVIOR

A. Fill Rate

The effect of fill rate on drainage is shown in Figure 18. A case with a very small fill time of 5 s is compared with cases with slower injection velocities corresponding to fill times of 120 s and 600 s (10 minutes). For the height of foam column and parameters considered, the drainage-time difference between filling in 5 s and 120 s is small. However, spaces for which HiEx foams are typically used for fire suppression have higher ceilings and thus the foam column heights are potentially taller by an order of magnitude. Hence, the fill times could be much larger. The curve corresponding to a 600s fill time shows a clear difference from the other curves; this difference cannot be predicted using a free-drainage model.

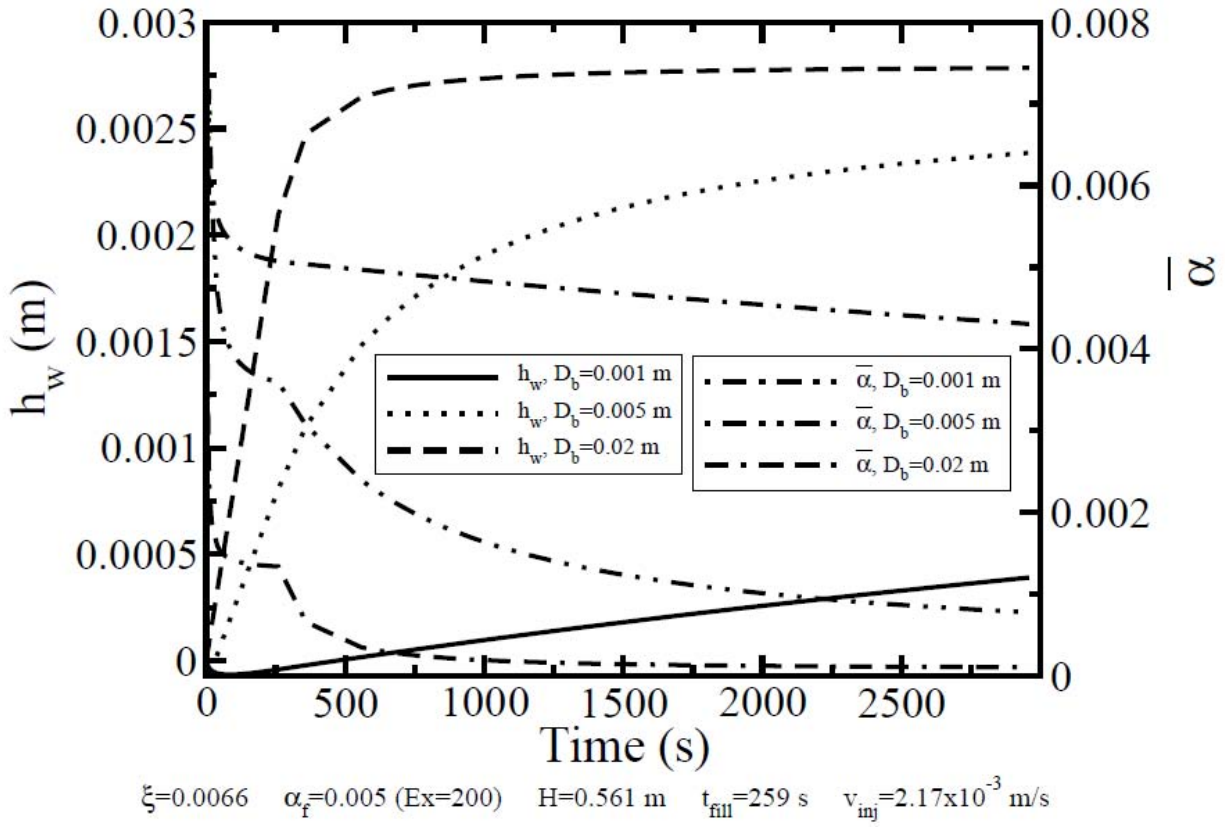

Figure 19: Effect of bubble size on drainage.

B. Bubble Size

The effect of the bubble size on drainage is shown in Figure 19. The model predicts that foams with larger bubbles drain at a faster rate and drain more liquid before reaching equilibrium. This effect has been observed in previous studies at lower expansion ratios near 20 and bubble sizes less than a millimeter [9]. At a given liquid fraction, a foam with larger bubbles will have channels with greater cross-sectional area. Because the average velocity in the channel is proportional to the channel area, the drainage rate from the foam will be greater.

In Figure 19, drainage is predicted for a bubble diameter of 0.001 m (1 mm). In studies of low-expansion foams, the bubble diameters are typically smaller. The model indicates that HiEx foams do not drain appreciably for these smaller bubble sizes. However, the foams used in practice for HiEx can have bubble diameters up to a few centimeters. As Figure 19 indicates, HiEx foams drain appreciably during and after the filling process for the bubble sizes used in practice.

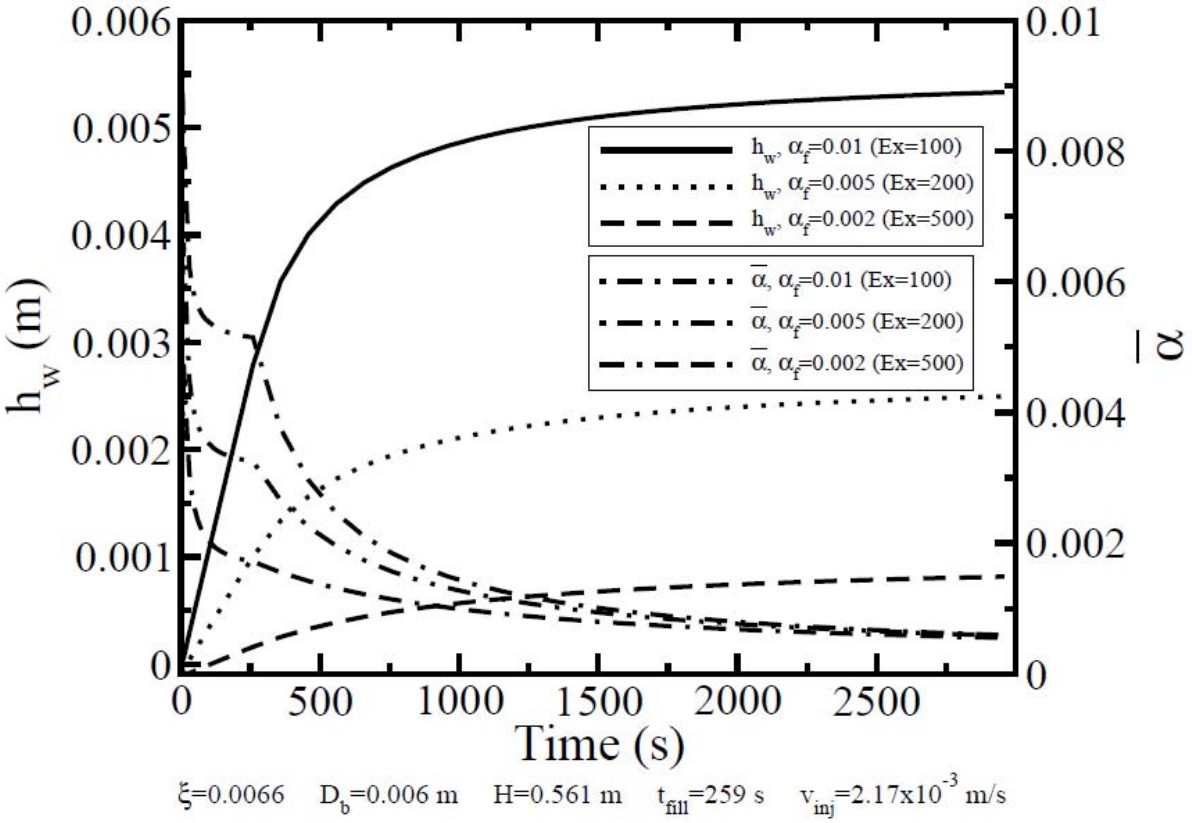

Figure 20: Effect of input expansion ratio on drainage.

C. Expansion Ratio

The effect of varying the expansion ratio of the input foam on drainage behavior is displayed in Figure 20. For a given bubble size, the area of the channels will decrease with increasing expansion ratio. The drainage rate is therefore reduced in foams with higher expansion ratios.

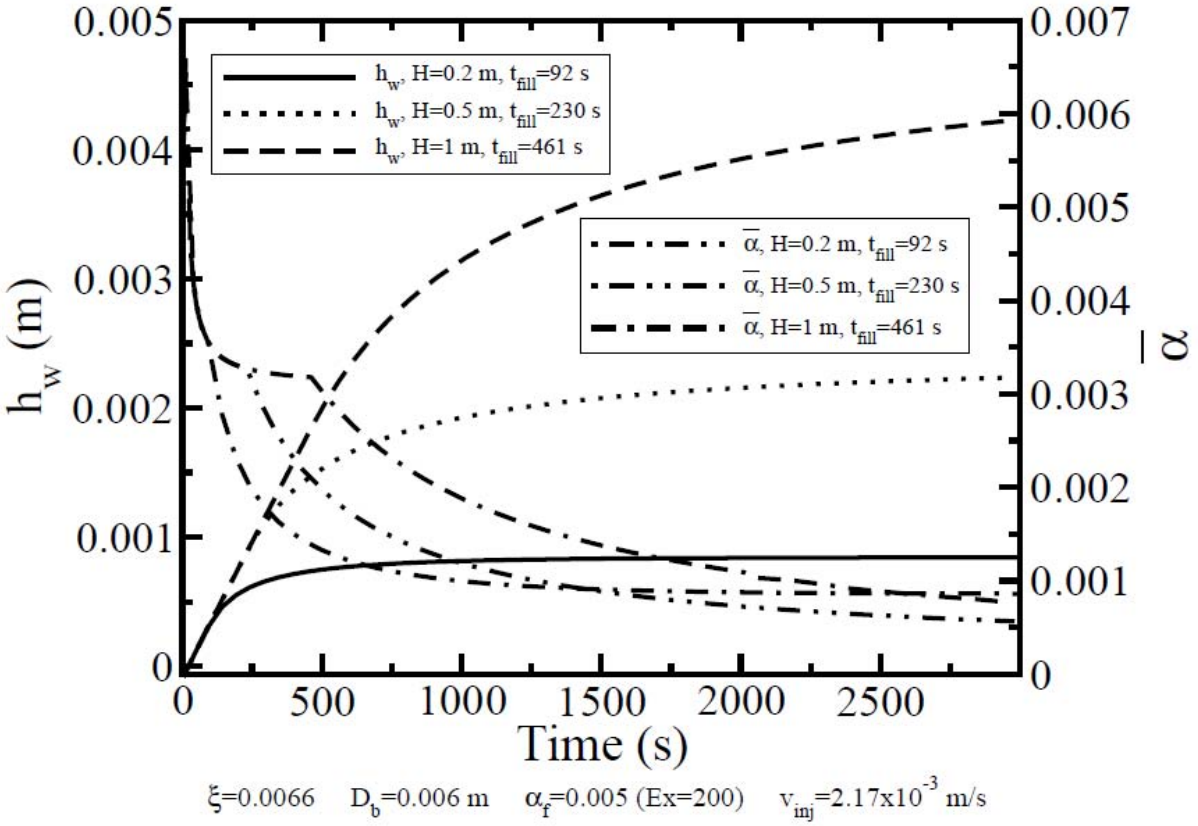

Figure 21: Effect of column height on drainage.

D. Column Height

The effect of column height on drainage is shown in Figure 21. As the height of the foam column increases, the time required to reach equilibrium also increases. Further, the liquid fraction at equilibrium also decreases with increasing column height. This behavior is caused by the pressure gradient of the model, which decreases with increasing column height. The effect of capillarity on the column will therefore be smaller for taller columns, allowing a greater percentage of liquid to drain before equilibrium is reached.

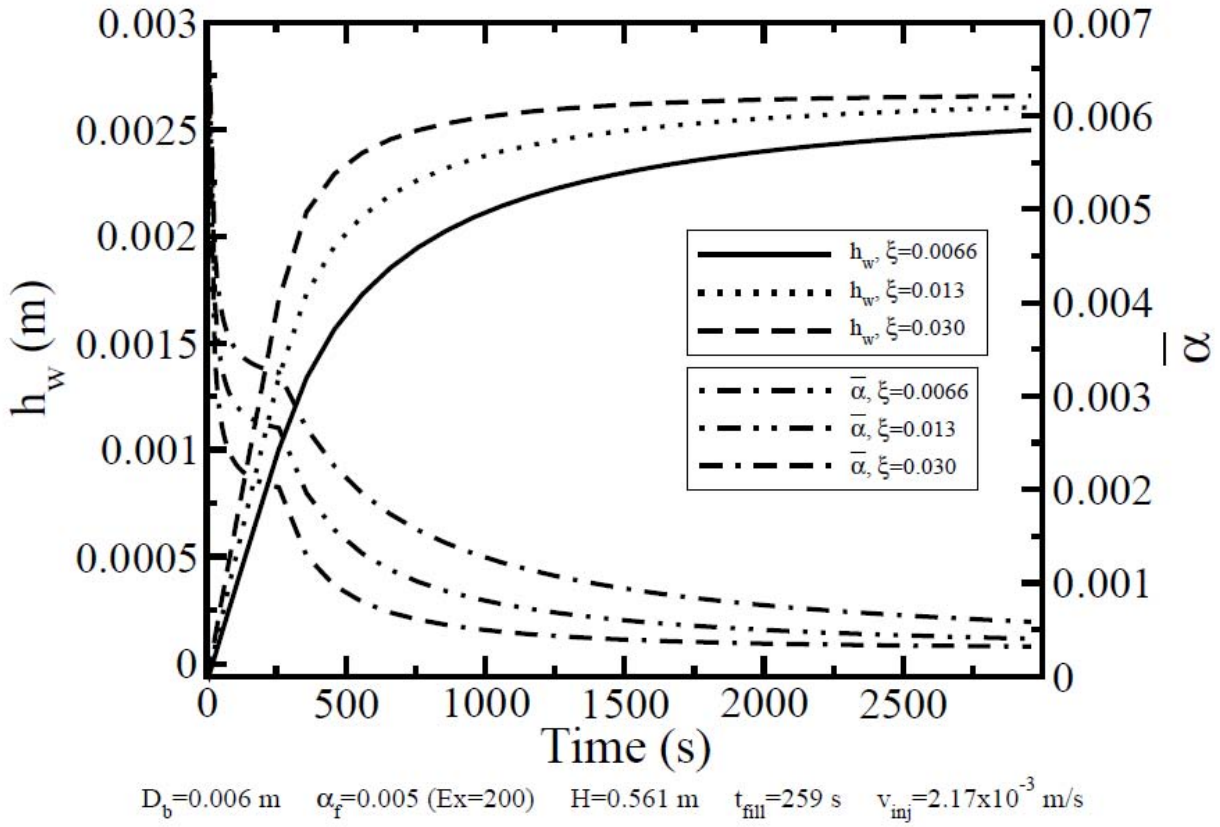

Figure 22: Effect of permeability coefficient on drainage.

E. Permeability Coefficient

The effect of varying the permeability coefficient on drainage is plotted in Figure 22. The drainage behavior for the permeability constant $\xi = 0.0066$ is shown along with greater values, 0.013 and 0.030. These values correspond approximately to conditions that have been reported in the literature. Koehler et al. [7] reported a calculated value of a permeability constant for channels with immobile walls, $\xi \approx 0.0063$, which is the similar in value to the permeability constant used in our work. Magrabi et al. [9] used a permeability coefficient of about 0.025 and 0.01 to model foams at an expansion ratio of 20 made from the surfactant solutions aqueous film-forming foam (AFFF) and film-forming fluoroprotein foam (FFFP), respectively.

5.0 CONCLUSIONS

We have developed a model to describe the loss of liquid from foam that includes an essential process of industrial foam applications: the process of filling a space with foam. The model solves for the time evolution of liquid drained from the foam and the average liquid

content within the foam. Introducing the filling process adds a new time scale, the fill time, to the drainage problem that has a significant effect on the drainage behavior.

An important aspect of the work is that approximations in the model equations that describe the drainage of liquid from foam are made to provide simple analytical solutions. The analytical solutions indicate that the drainage rate remains constant during the filling process and, after filling, decays exponentially.

The investigation is aimed at describing drainage from foams with very low liquid content, such as those used in high-expansion (HiEx) foam fire-suppression applications. Model results are in good agreement with the experimental data from bench-scale experiments on HiEx foams. Although numerical solutions were needed for the model equations to obtain sufficient accuracy under the bench-scale conditions, the simple analytical solutions of the model are shown to be valid for field conditions.

Modeling predictions were compared with experimental data using a permeability coefficient, $\xi = 5.1\times10^{-3}$, that was calculated from the permeability derived in Ref. [7] for a no-slip condition at the channel walls. The model was fit to experimental data by adjusting the bubble size. The bubble size that provided the best fit to experiment results was within the bubble-size distribution obtained by photographs of the experimental foams. Fill rate, bubble size, input-foam expansion ratio, column height, and permeability coefficient each have a substantial impact on the foam drainage behavior predicted by the model.

6.0 ACKNOWLEDGMENTS

This work was funded by the Office of Naval Research through the Naval Research Laboratory.

7.0 REFERENCES

[1] R. A. Leonard and R. Lemlich, A.I.Ch.E. Journal **11**, 18 (1965).

[2] D. Desai and R. Kumar, Chem Eng. Sci. **37**, 1361 (1982).

[3] D. Desai and R. Kumar, Chem. Eng Sci. **38**, 1525 (1983).

[4] M. V. Ramani, R. Kumar, and K. S. Gandhi, Chem. Eng. Sci. **48**, 455 (1993).

[5] K. Podual, R. Kumar, and K. S. Gandhi, Chem. Eng. Sci. **51**, 1393 (1996).

[6] G. Verbist, D. Weaire, and A. M. Kraynik, J. Phys.: Condens. Matter **8**, 3715 (1996).

[7] S. Koehler, S. Hilgenfeldt, and H. A. Stone, Langmuir **16**, 6327 (2000).

[8] S. A. Magrabi, B. Z. Dlugogorski, and G. J. Jameson, AIChE Journal **47**, 314 (2001).

[9] S. A. Magrabi, B. Z. Dlugogorski, and G. J. Jameson, Fire Safety Journal **37**, 21 (2002).

[10] A. Bhakta and E. Ruckenstein, Langmuir **11**, 1486 (1995).

[11] R. J. Germick, A. S. Rehill, and G. Narsimhan, J. Food Eng. **23**, 555 (1994).

[12] M. Durand, G. Martinoty, and D. Langevin, Phys. Rev. E **60**, R6307 (1999).

[13] V. Carrier and A. Colin, Langmuir **19**, 4535 (2003).

[14] V. Carrier, S. Destouesse, and A. Colin, Phys. Rev. E **65**, 061404 (2002).

APPENDIX A: Calculation of the superficial liquid velocity for a cylindrical channel

In order to treat liquid flow in foam, we first assume the foam is composed of a network of cylindrical channels. We calculate the superficial liquid velocity for a cylindrical channel to show its dependence on the channel area. In the calculation, we consider steady-state flow. Also, we assume that the walls are immobile, i.e. there is a no-slip condition at the surface of the channels. This gives rise to a parabolic velocity profile. The velocity of the liquid within the channel at a distance r from the axis can be described by the equation

$$v_z = v_{max}\left[1-\frac{r}{r_p}\right] \tag{67}$$

where r_p is the radius of the channel.

The stress at a distance r is given by

$$\tau_{rz} = -\mu\frac{\partial v_z}{\partial r} = -\mu\frac{\partial}{\partial r}\left[v_{max}\left(1-\frac{r}{r_p}\right)\right] = \frac{2\mu r v_{max}}{r_p^2} \quad . \tag{68}$$

We are interested in modeling the stress at the surface of the channel as an interaction between phases in the multiphase momentum equation. Hence, we want the value of the stress at $r = r_p$

$$\tau_{rz}(r_p) = \frac{2\mu v_{max}}{r_p} \quad . \tag{69}$$

We must calculate the force from this stress by integrating over the surface area of the channel

$$F_{rz} = \int \tau_{rz}\, dA = \frac{2\mu v_{max}}{r_p}\left[2\pi r_p L\right] = 4\pi\mu v_{max} L \tag{70}$$

where $2\pi r_p L$ is the surface area of the channel. Eq. (70) gives the force in a single channel. In order to find the total force per unit volume of the simplified foam, we need to multiply by the number of channels per unit volume.

For dodecahedral geometry, there are $n_p = 10$ channels per bubble. For this case, the frictional force per unit volume, $\tilde{F}_f$, is

$$\tilde{F}_f = F_{rz} n_p \tilde{N}_b = 10 F_{rz} \tilde{N}_b \tag{71}$$

where $\tilde{N}_b$ is the number of bubbles per unit volume. We can calculate the total number of bubbles, N_b, by

$$N_b = \frac{V_f}{V_b} \tag{72}$$

where V_f is the total volume of the foam and V_b is the volume per bubble. Dividing the previous expression by V_f yields

$$\tilde{N}_b = \frac{1}{V_b} = \frac{1}{\frac{1}{4}\left(15+7\sqrt{5}\right)L^3} \quad . \tag{73}$$

The force per unit volume due to friction at the surface of the channels is therefore

$$\tilde{F}_f = n_p \tilde{N}_b F_{rz} = \left(\frac{10}{\frac{1}{4}\left(15+7\sqrt{5}\right)L^3} \right) \left[4\pi\mu v_{max} L \right] = \frac{160\pi\mu v_{max}}{\left(15+7\sqrt{5}\right)L^2} \quad . \tag{74}$$

We want to model this frictional force as an interaction between phases in the liquid-phase momentum equation. The momentum equation, ignoring the inertial and accumulation terms, for the liquid phase (denoted by l) within a two-phase mixture including gas (denoted by a) is given by

$$0 = -\nabla P^{(l)} - \left[\nabla \cdot \underline{\underline{\tau}} \right]^{(l)} + \rho^{(l)} \mathbf{g} + \rho^{(l)} F^{la} \left(v_a - v_l \right) \tag{75}$$

where $\rho^{(l)} = \alpha\rho$ is the effective density of the liquid within the mixture and $P^{(l)} = \alpha P_l$ is the effective liquid pressure. The last term in the previous expression is the interaction between the gas and liquid phases, and this is the term for which we want to model the friction between liquid and gas in a foam using $\tilde{F}_f = \rho^{(l)} F^{la} \left(v_a - v_l \right)$. The quantity F^{la} is termed a time constant for the interaction between the phases. The interaction term has the form

$$-\alpha\rho F^{la} v_s = \frac{160\pi\mu v_{max}}{\left(15+7\sqrt{5}\right)L^2} \tag{76}$$

when we consider the gas velocity $v_a = 0$. We also express the liquid velocity in terms of the superficial velocity, v_s. To relate v_{max} to v_s, let us consider the pore velocity, v_p, which is the average liquid velocity within a channel. The average velocity, v_p, is related to the maximum velocity, v_{max}, by a constant; let us make the relation

$$v_{max} = c v_p \quad . \tag{77}$$

We are considering steady-state flow in cylindrical channels, and therefore $c = 2$ for the resulting parabolic velocity profile. We also must relate the channel velocity to the superficial velocity. We achieve this by means of a mass balance in a foam column at the interface between a foam and liquid layers. Let us denote N_p as the total number of channels that are connected and drain directly to the foam layer, each having a flow rate of $a_p v_p$. The liquid drained from the foam causes the liquid layer to rise, and the flow rate of the liquid is $v_s A$, where A is the cross-sectional area of the foam column. Balancing these flow rates, we have the relation

$$N_p a_p v_p = v_s A \quad \Rightarrow \quad v_p = \left(\frac{A}{N_p a_p} \right) v_s \quad . \tag{78}$$

A common equation in porous media is $v_s = \epsilon v_p$, where ϵ is the porosity of the medium. If we consider foam as a porous media with liquid filling the pores, then $\epsilon = \alpha$. This allows the relation $\alpha = N_p a_p / A$. The time constant is therefore

$$F^{la} = \frac{-160\pi\mu c}{\left(15+7\sqrt{5}\right)L^2} \left(\frac{1}{\rho\alpha} \right) \left(\frac{A}{N_p a_p} \right) \quad . \tag{79}$$

Our momentum equation for the liquid phase is

$$0 = -\nabla P^{(l)} + \rho\alpha\mathbf{g} - \frac{160\pi\mu c}{\left(15+7\sqrt{5}\right)L^2} \left(\frac{A}{N_p a_p} \right) v_s \quad . \tag{80}$$

Solving for v_s yields

$$v_s = \left[\left(\frac{\left(15+7\sqrt{5}\right)L^2}{160\pi\mu c} \right) \left(\frac{N_p a_p}{A} \right) \right] \left(\rho\alpha\mathbf{g} - \nabla P^{(l)} \right) \quad . \tag{81}$$

If we set $N_p a_p / A = \alpha$, then

$$v_s = \left[\left(\frac{\left(15+7\sqrt{5}\right)}{160\pi\mu c} \right) \alpha^2 L^2 \right] \left(\rho\mathbf{g} - \frac{\nabla(\alpha P_l)}{\alpha} \right) \quad . \tag{82}$$

The superficial velocity in terms of Darcy's law is given by

$$v_s = \frac{k}{u} \left(\rho g - \nabla P_l \right) \quad . \tag{83}$$

Assuming that $\nabla(\alpha P_l)/\alpha \approx \nabla P_l$, the previous expression can be used to find the permeability of the foam with cylindrical cross-section using Eq. (82), yielding

$$k = \left(\frac{\left(15+7\sqrt{5}\right)}{160\pi\mu c} \right) \alpha^2 L^2 \quad . \tag{84}$$

This shows that the permeability (and the superficial velocity) is proportional to the square of α. The permeability constant for this case is

$$\xi = \left(\frac{\left(15+7\sqrt{5}\right)}{160\pi c} \right) \approx 0.03 \quad . \tag{85}$$

The case considered here is for vertically oriented cylindrical channels with immobile walls. By considering the equation for Hagen-Poiseuille flow in a cylindrical channel

$$v = \frac{a_p}{8\pi} \frac{\partial P}{\partial z} \qquad (cylindrical) \tag{86}$$

and the equation for flow in a channel with equilateral-triangular cross section derived by Desai and Kumar

$$v = \frac{a_p}{20\sqrt{3}} \frac{\partial P}{\partial z} \qquad (equilateral \;\; triangular) \quad , \tag{87}$$

we calculate a correction factor, $8\pi / 20\sqrt{3} \approx 0.726$, that can correct the value in Eq. (85) for vertically oriented cylindrical channels to yield ξ for vertically oriented channels with equilateral triangular cross section:

$$\xi \approx 0.03 \times 0.726 \approx 0.022 \qquad (equilateral \;\; triangular) \quad . \tag{88}$$

The channels in foam have a cross-sectional area that is shaped like a triangle wherein the three edges are curved in a concave manner, i.e. a scalloped-triangular shape. We expect that the value of ξ for vertically oriented channels with scalloped-triangular cross section and immobile walls is slightly less than the value provided in Eq. (88).

APPENDIX B: Parameters for comparison with Reference [8].

The following parameters were used to compare the model in this work with the model calculations reported in Ref. [8] as shown in Figure 13 and Figure 14.

γ	Surface tension	$2.25\times10^{-2}\ \frac{N}{m}$
μ	Liquid viscosity	$8.94\times10^{-4}\ \frac{kg}{m\,s}$
ξ	Permeability constant	0.0245
L	Plateau border length Note: $L = 0.408 D_b$	$1.09\times10^{-4}\ m$ $\left(D_b = 2.66\times10^{-4}\ m\right)$
		$2.20\times10^{-4}\ m$ $\left(D_b = 5.40\times10^{-4}\ m\right)$
ρ	Liquid density	$997\ \frac{kg}{m^3}$
H	Column height	$0.2\ m$
$\alpha_f\ (=\alpha_0)$	Liquid fraction of input foam	0.05
α_w	Liquid fraction at foam/liquid interface (mass balance)	1
α_w	Liquid fraction at foam/liquid interface (momentum balance)	0.26
t_0	Starting time	$0\ s$